Computational and Applied Mathematics (2020) 39:142
https://doi.org/10.1007/s40314-020-01169-9

# Compact finite-difference method for 2D time-fractional convection–diffusion equation of groundwater pollution problems

**Lingyu Li**[1,2] · **Ziwen Jiang**[1] · **Zhe Yin**[1]

Received: 14 July 2019 / Revised: 5 March 2020 / Accepted: 16 April 2020


**Abstract**
In this work, we provide a compact finite-difference scheme (CFDS) of 2D time-fractional convection–diffusion equation (TF-CDE) for solving fluid dynamics problem, especially groundwater pollution. The successful predication of the pollutants concentration in groundwater will greatly benefit the protection of water resources for provide the fast and intuitive decision-makings in response to sudden water pollution events. Here, we creatively use the dimensionality reduction technology (DRT) to rewrite the original 2D problem as two equations, and we handle each one as a 1D problem. Particularly, the spatial derivative is approximated by fourth-order compact finite-difference method (CFDM) and time-fractional derivative is approximated by $L_1$ interpolation of Caputo fractional derivative. Based on the approximations, we obtain the CFDS with fourth-order in spatial and $(2-\alpha)$-order in temporal by adding two 1D results. In addition, the unique solvability, unconditional stability, and convergence order $\mathcal{O}(\tau^{2-\alpha}+h_1^4+h_2^4)$ of the proposed scheme are studied. Finally, several numerical examples are carried out to support the theoretical results and demonstrate the effectiveness of the CFDS based DRT strategy. Obviously, the method developed in 2D TF-CDE of groundwater pollution problem can be easily extended for the other complex problems.

**Keywords** Compact finite-difference method · Time-fractional convection–diffusion equation · Groundwater pollution · Stability and convergence · Numerical examples

**Mathematics Subject Classification** 65M06 · 65M12 · 65M15 · 65M22 · 35R11

Communicated by José Tenreiro Machado.

✉ Ziwen Jiang
ziwjiang@163.com

✉ Zhe Yin
zyin_sdnu@163.com

Lingyu Li
sdnully2012@163.com

[1] School of Mathematics and Statistics, Shandong Normal University, Jinan 250014, China

[2] School of Control Science and Engineering, Shandong University, Jinan 250061, China

Published online: 18 May 2020

## 1 Introduction

Convection–diffusion equation (CDE) has been recommended to illustrate many quantities such as mass, velocity, vorticity, heat, energy, and so on Logan and Zlotnik (1995), Sari et al. (2010), NeZheng (2014) and Qiu and Shi (2016). The solution of CDE plays an important role in various fields of science; for example, gas transport in heterogeneous soil and gas reservoirs (Chang et al. 2018), contaminant diffusion in complex geological formations (Wang and Ewing 1995; Cortis et al. 2004), contaminant transport in groundwater (Sun and Yeh 1983; Ewing and Wang 1994; Li et al. 2020), spread of pollutants in rivers (Ercan 2020), contaminant dispersion in shallow lakes and reservoirs (Kinzelbach 1990), heat conduction phenomenon in Physics (Cao et al. 2018), relaxation in polymer systems in Chemistry (Munyakazi 2015), dynamics of protein molecules in Biology, and image denoising in Biomedical (Shih et al. 2009). Analytic solution of some CDEs can be found in some special cases (Yadav et al. 2010; Günerhan 2020), but it turns out to be very difficult to get the analytic solution of most CDEs (Yu et al. 2019). These CDE models are solved, in general, using numerical techniques. In the past decades, the research of numerical method of CDE is very eye-catching (Sun 1989; Liang and Zhao 1997; Rap et al. 2007; Gong et al. 2018).

In recent years, fractional CDEs have received more and more attention and have been used to a wide range of problems in anomalous diffusion, fluid flow, electrostatics, fractal theory, quantum economy, signal processing, and system recognition (Li and Zeng 2012). TF-CDE, as a class of fractional CDEs, is particularly important in reflecting some critical features in contaminant transport through complex porous media like heavy-tail decay, early breakthrough of contaminant, and scale-dependent coefficients (Sun et al. 2013). More recently, a variety of numerical methods for TF-CDE have been proposed such as the finite-element method (FEM) (Jin et al. 2016; Chen et al. 2019), discontinuous Galerkin (DG) method (Xu and Hesthaven 2014), finite-difference method (FEM) (Zhu et al. 2012), the collocation method (Zhou and Xu 2016), the spectral method (Li and Xu 2009), coupled method (Taghavi et al. 2017), etc., to name just a few. The FEM is the oldest, but still remains widely used in hydrogeological practice (Kovarik 2000). The key issue of the design of efficient numerical scheme for TF-CDEs is computational accuracy, and CFEM is one of the most popular methods (Mohebbi and Abbaszadeh 2013; Wang and Vong 2014; Cui 2015; Zhang et al. 2018; Wu and Zhai 2019).

Groundwater pollution is an important topic of environmental sciences. At present, the studies on groundwater pollution problems are mainly divided into two categories. On one hand, numerical simulation software of groundwater system, such as geographic information system (GIS), has been developed and used to monitor pollution diffusion because of its modularity, visualization, and interaction (Srivastava et al. 2012; Subramani and Krishnamurthi 2014; Esquivel et al. 2015; Machiwal et al. 2018). On the other hand, mathematical models, formulated by a nonlinear initial boundary-value problem (IBVP) of partial differential equation (PDE), are the effective tool to solve different tasks predicting pollutant movement (Fried 1975; Yuan et al. 2019). For instance, (Wang and Ewing 1995) developed a Eulerian–Lagrangian localized adjoint methods (ELLAM) to solve variable–coefficient advective–diffusive–reactive (ADR) transport equations governing contaminant transport in groundwater owing through a porous medium. (Smaoui et al. 2008) presented a total variation diminishing (TVD) method to discrete the advection–diffusion equation of contaminant migration in a 2D horizontal aquifer. (Winkler et al. 2015) provide a comparative study of three different methods simulating CDEs regarding groundwater pollution. (Augeraud-Véron et al. 2017) considered an optimal control problem of groundwater pollution governing

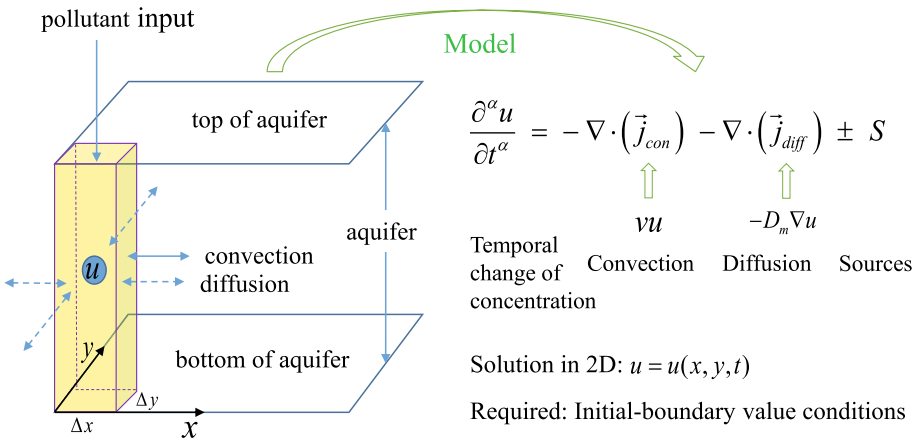


**Fig. 1** Pollution transport processes and its mathematics model

by convection–diffusion–reaction equation in a 3D domain. (Ercan 2020) studied the self-similarity in transport of groundwater contaminants based on 3D ADR transport equation with various initial boundary-value conditions.

Numerical simulation of the groundwater pollution problem in 2D horizontal regional flow is discussed in this paper. The pollution transport processes, represented by Fig. 1, is modeled by the 2D TF-CDE with seepage only in $x$-axis direction. Figure 1 not only describes the phenomenon of slow-diffusion of groundwater pollution problems, but also shows its corresponding mathematical model, where $u$ is the concentrations, $\overrightarrow{v}$ is the convection velocity along the $x$-axis, and $D_m$ is the diffusion coefficient in $x$-axis and $y$-axis direction. This means that there is an initial amount of pollution at the source which will be distributed in $x$-axis direction during time. The related problem has been researched by (Sun 1989; Li et al. 2013; Winkler et al. 2015; Li and Yin 2017; Li et al. 2018; Günerhan 2020). However, these literatures only researched on the case of integer order CDE, or the proposed methods are convergent only with the second-order accuracy in spatial. (Li and Yin 2017) researched the integer-order problem with the general second-order FEM. The discussion of its high-order scheme with fractional order has not been done before, to make up for it and obtain more accurate concentration of groundwater pollutants at different time $t$ and location $(x, y)$, we consider a kind of high-order CFDM by DRT, so that the spatial accuracy is improved to the fourth order. DRT avoids the non-square matrix problem caused by the action of compact operator acting in the $x$ and $y$ directions. Different from the ADI method, the coefficient matrix formed by DRT is a nine-diagonal sparse matrix, ones only need to solve one linear algebraic equation system, and do not need the middle layer.

The paper is organized as follows: In Sect. 2, we transform original equation into two TF-CDE by DRT equivalently, and then discretize the equivalent form with one-dimensional TF-CDE using CFDM approximation for spatial derivatives so as to present a fourth-order CFDS, and time-fractional derivative is approximated by $L_1$ interpolation of Caputo fractional derivatives. In Sect. 3, the matrix form for the proposed scheme is given, and we also discussed about the solving methods for the linear system of equations. In Sect. 4, unique solvability of proposed scheme is given by analyzing eigenvalues of its matrix form. In Sect. 5, we prove that the scheme is unconditionally stable. In particular, the convergence analysis is shown in Sect. 6 with order $\mathcal{O}(\tau^{2-\alpha} + h_1^4 + h_2^4)$, in which $0 < \alpha < 1$. Finally,

numerical examples are carried out in Sect. 7 to show that the scheme can improve the spatial accuracy significantly in simulating pollutant diffusion concentration. The paper concludes with a summary in Sect. 8.

## 2 Fourth-order compact finite-difference scheme (CFDS)

In this paper, for simulating the case of an instantaneous release of pollution, we consider the following TF-CDE of groundwater pollution problem shown in Fig. 1 on the rectangular region $\Omega = (0, l_1) \times (0, l_2)$:

$$\frac{\partial^\alpha u(x,y,t)}{\partial t^\alpha} - \left( D_1 \frac{\partial^2 u(x,y,t)}{\partial x^2} + D_2 \frac{\partial^2 u(x,y,t)}{\partial y^2} \right) + v \frac{\partial u(x,y,t)}{\partial x} = g(x,y,t), \tag{2.1}$$

where $(x, y) \in \Omega$, $t \in (0, T]$, $D_1$, and $D_2$ are two positive diffusion coefficients directing $x$-axis direction and $y$-axis direction, respectively. $v$ is a positive constant representing the convection velocity of the contaminant along the $x$-axis, $g(x, y, t)$ is the source term. $\alpha \in (0, 1)$ refers to the order of time-fractional derivative, and (2.1) becomes a integer-order convection–diffusion problem when $\alpha = 1$.

For (2.1), the boundary value and initial value conditions are given by:

$$\begin{cases} u(0,y,t) = \psi_1(y,t), & u(l_1,y,t) = \psi_2(y,t), & y \in (0,l_2),\ t > 0, \\ u(x,0,t) = \phi_1(x,t), & u(x,l_2,t) = \phi_2(x,t), & x \in (0,l_1),\ t > 0, \\ u(x,y,0) = \varphi(x,y), & & (x,y) \in \Omega. \end{cases} \tag{2.2}$$

Clearly, these boundary value conditions are satisfied with the consistency conditions:

$$\begin{aligned} &\psi_1(0,t) = \phi_1(0,t), \quad \phi_1(l_1,t) = \psi_2(0,t), \\ &\psi_2(l_2,t) = \phi_2(l_1,t), \quad \phi_2(0,t) = \psi_1(l_2,t). \end{aligned} \tag{2.3}$$

Obviously, (2.1), (2.2), and (2.3) construct the IBVP of 2D TF-CDE. To some extent, solving the IBVP accurately can provide suggestions for government departments to deal with groundwater pollution problems. Here, we are going to study the CFDM for solving it.

### 2.1 Mesh partition and some notations

Take two positive integers $N_1$ and $N_2$, the spatial step sizes are noted as $h_1 = \frac{l_1}{N_1}$, $h_2 = \frac{l_2}{N_2}$, and the grid nodes are denote by $x_i = ih_1 (i = 0, 1, 2, ..., N_1)$, $y_j = jh_2 (j = 0, 1, 2, ..., N_2)$. Take a positive integer $K$ again, the temporal step size is marked $\tau = \frac{T}{K}$ and $t_k = k\tau$, where $k = 1, 2, ..., K$.

Let $\bar{\Omega}_h = \{(x_i, y_j) | 0 \le i \le N_1, 0 \le j \le N_2\}$, $\Omega_h = \bar{\Omega}_h \cap \Omega$, $\partial\Omega_h = \bar{\Omega}_h \cap \partial\Omega$, $\omega = \{(i, j) | (x_i, y_j) \in \Omega_h\}$, $\partial\omega = \{(i, j) | (x_i, y_j) \in \partial\Omega_h\}$, $\bar{\omega} = \omega \cup \partial\omega$, $\Omega_\tau = \{t_k | 0 \le k \le K\}$. Denote the grid function space $\mathbb{U}_h = \{u_{ij} \big| (i, j) \in \bar{\omega}\}$ on $\bar{\Omega}_h$, for $\forall\, u_{ij} \in \mathbb{U}_h$, we introduce some notations that will be used later:

$$\delta_x u_{ij}^k = \frac{u_{i+1,j}^k - u_{i-1,j}^k}{2h_1}, \quad \delta_x^2 u_{ij}^k = \frac{u_{i+1,j}^k - 2u_{ij}^k + u_{i-1,j}^k}{h_1^2}, \quad \delta_y^2 u_{ij}^k = \frac{u_{i,j+1}^k - 2u_{ij}^k + u_{i,j-1}^k}{h_2^2}. \tag{2.4}$$

At last, we define:

$$u_{ij}^k = u(x_i, y_j, t_k), \quad g_{ij}^k = g(x_i, y_j, t_k), \tag{2.5}$$

where $(i, j) \in \bar{\omega},\ 0 \le k \le K$.

### 2.2 $L_1$ interpolation approximation for Caputo fractional derivative

In our work, the time-fractional derivative $\frac{\partial^\alpha u(x,y,t)}{\partial t^\alpha}$ in (2.1) will be as taken as Caputo fractional derivative (see Li et al. 2012; Mohebbi and Abbaszadeh 2013) as follows:

$$\frac{\partial^\alpha u(x, y, t)}{\partial t^\alpha} = {}_0^C D_t^\alpha u(x, y, t) = \frac{1}{\Gamma(1-\alpha)} \int_0^t \frac{\partial u(x, y, s)}{\partial s} \frac{ds}{(t-s)^\alpha}, \tag{2.6}$$

where $\Gamma(\cdot)$ refers to the gamma function.

We consider the $L_1$ interpolation approximation of Caputo fractional derivative in condition of $\alpha$ $(0 < \alpha < 1)$:

$$\begin{aligned} {}_0^C D_t^\alpha u(x, y, t)\Big|_{t=t_k} &= \frac{1}{\Gamma(1-\alpha)} \int_0^{t_k} \frac{\partial u(x, y, s)}{\partial s} \frac{ds}{(t_k - s)^\alpha} \\ &= \frac{1}{\Gamma(1-\alpha)} \sum_{m=1}^{k} \int_{t_{m-1}}^{t_m} \frac{\partial u(x, y, s)}{\partial s} \frac{ds}{(t_k - s)^\alpha}. \end{aligned} \tag{2.7}$$

Making the linear interpolation for $u(x, y, s)$ on interval $[t_{m-1}, t_m]$, it shows:

$$L_{1,m} u(x, y, s) = \frac{t_m - s}{\tau} u(x, y, t_{m-1}) + \frac{s - t_{m-1}}{\tau} u(x, y, t_m), \tag{2.8}$$

$$u(x, y, s) - L_{1,m} u(x, y, s) = \frac{1}{2} u''(x, y, \xi_m)(s - t_{m-1})(s - t_m), \quad s \in [t_{m-1}, t_m], \tag{2.9}$$

where $\xi = \xi_m(s) \in (t_{m-1}, t_m)$. Using $L_{1,m} u(x, y, s)$ to approximate $u(x, y, s)$ in (2.7), it derives:

$$\begin{aligned} &{}_0^C D_t^\alpha u(x, y, t)\Big|_{t=t_k} \\ &\approx \frac{1}{\Gamma(1-\alpha)} \sum_{m=1}^{k} \int_{t_{m-1}}^{t_m} \frac{u(x, y, t_m) - u(x, y, t_{m-1})}{\tau} \cdot \frac{1}{(t_k - s)^\alpha} \mathrm{d}s \\ &= \frac{1}{\Gamma(1-\alpha)} \sum_{m=1}^{k} \frac{u(x, y, t_m) - u(x, y, t_{m-1})}{\tau} \cdot \int_{t_{m-1}}^{t_m} \frac{1}{(t_k - s)^\alpha} \mathrm{d}s \\ &= \frac{1}{\Gamma(1-\alpha)} \sum_{m=1}^{k} \frac{u(x, y, t_m) - u(x, y, t_{m-1})}{\tau} \cdot \frac{1}{1-\alpha} \Big[ (t_k - t_{m-1})^{1-\alpha} - (t_k - t_m)^{1-\alpha} \Big] \\ &= \frac{\tau^{-\alpha}}{\Gamma(2-\alpha)} \sum_{m=1}^{k} \Big[ u(x, y, t_m) - u(x, y, t_{m-1}) \Big] \cdot \Big[ (k - m + 1)^{1-\alpha} - (k - m)^{1-\alpha} \Big] \end{aligned}$$

$$= \frac{\tau^{-\alpha}}{\Gamma(2-\alpha)} \sum_{m=1}^{k} b_{k-m}^{(\alpha)} \Big[ u(x, y, t_m) - u(x, y, t_{m-1}) \Big]$$

$$s = \frac{\tau^{-\alpha}}{\Gamma(2-\alpha)} \Big[ b_0^{(\alpha)} u(x, y, t_k) - \sum_{m=1}^{k-1} \big( b_{k-m-1}^{(\alpha)} - b_{k-m}^{(\alpha)} \big) u(x, y, t_m) - b_{k-1}^{(\alpha)} u(x, y, t_0) \Big], \tag{2.10}$$

where

$$b_l^{(\alpha)} = (l+1)^{1-\alpha} - l^{1-\alpha}, \qquad l \geq 0. \tag{2.11}$$

Therefore, we obtain the approximation formula to compute ${}_0^C D_t^{\alpha} u(x, y, t)|_{t=t_k}$:

$$D_{\tau}^{\alpha} u(x, y, t_k) := \frac{\tau^{-\alpha}}{\Gamma(2-\alpha)} \Big[ b_0^{(\alpha)} u(x, y, t_k) - \sum_{m=1}^{k-1} \big( b_{k-m-1}^{(\alpha)} - b_{k-m}^{(\alpha)} \big) u(x, y, t_m) - b_{n-1}^{(\alpha)} u(x, y, t_0) \Big]. \tag{2.12}$$

(2.12) is the $L_1$ interpolation approximation formula ($L_1$ formula) for the Caputo fractional derivative. In particular, the coefficient $b_l^{(\alpha)}$ has the following properties:

**Lemma 2.1** (Sun and Gao 2015) *Let $\alpha \in (0, 1)$, $b_l^{(\alpha)}$ is defined by the Eq. (2.11), $l = 0, 1, 2, \ldots$, and then, we have:*

(1) $1 = b_0^{(\alpha)} > b_1^{(\alpha)} > b_2^{(\alpha)} > \cdots > b_l^{(\alpha)} > 0; \quad b_l^{(\alpha)} \to 0 \ (l \to \infty);$

(2) $(1-\alpha) l^{-\alpha} < b_{l-1}^{(\alpha)} < (1-\alpha)(l-1)^{-\alpha}, \quad l \geq 1.$

Lin and Xu (2007) and Gao et al. (2014) prove that the $L_1$ formula has a numerical precision of $(2-\alpha)$-order using different techniques. Here, we only give one conclusion from (Sun and Gao 2015) to illustrate it.

**Lemma 2.2** (Sun and Gao 2015) *Let $f(t) \in C^2[t_0, t_k]$; define:*

$$R(f(t_k)) = {}_0^C D_t^{\alpha} f(t)|_{t=t_k} - D_{\tau}^{\alpha} f(t_k),$$

*then we have:*

$$|R(f(t_k))| \leq \frac{1}{2\Gamma(1-\alpha)} \Big[ \frac{1}{4} + \frac{\alpha}{(1-\alpha)(2-\alpha)} \Big] \max_{t_0 \leq t \leq t_k} |f''(t)| \tau^{2-\alpha}. \tag{2.13}$$

### 2.3 Derivation of compact finite-difference scheme (CFDS)

In this section, we will use the fourth-order CFDS introduced by Li et al. (2018), Mohebbi and Abbaszadeh (2013) and Wang and Vong (2014) to discrete the spatial derivative terms in (2.1). Before that, we give a lemma at first.

**Lemma 2.3** (Mohebbi and Abbaszadeh 2013) *Consider the following differential equation:*

$$\eta \frac{d^2 y(x)}{dx^2} - \beta \frac{dy(x)}{dx} = f(x), \qquad 0 < x < L, \tag{2.14}$$

*with boundary conditions:*

$$y(0) = y_0, \quad y(L) = y_L.$$

*A three-point fourth-order CFDS for the equation is given as:*

$$\Big(\eta+\frac{\beta^2h^2}{12\eta}\Big)\delta_x^2y_i-\beta\delta_xy_i=f_i+\frac{h^2}{12}\Big(\delta_x^2f_i-\frac{\beta}{\eta}\delta_xf_i\Big)+O(h^4),\qquad 0<x<L, \tag{2.15}$$

*where L is a positive constant and:*

$$\delta_x^2y_i=\frac{y_{i+1}-2y_i+y_{i-1}}{h^2},\qquad \delta_xy_i=\frac{y_{i+1}-y_{i-1}}{2h}. \tag{2.16}$$

Considering that (Mohebbi and Abbaszadeh 2013) has gave a strict proof of the lemma, we will not go into details here. Then, we introduce the general notation to be used throughout the article:

$$w(x,y,t)=\frac{1}{\Gamma(1-\alpha)}\int_0^t\frac{\partial u(x,y,s)}{\partial s}\frac{\mathrm{d}s}{(t-s)^\alpha}. \tag{2.17}$$

Combined with (2.17), similar to the method in Li et al. (2018), (2.1) can be rewritten into two equations equivalently using the idea DRT:

$$-D_1\frac{\partial^2u(x,y,t)}{\partial x^2}+v\frac{\partial u(x,y,t)}{\partial x}=g(x,y,t)-w(x,y,t)+D_2\frac{\partial^2u(x,y,t)}{\partial y^2}, \tag{2.18}$$

$$-D_2\frac{\partial^2u(x,y,t)}{\partial y^2}=g(x,y,t)-w(x,y,t)+D_1\frac{\partial^2u(x,y,t)}{\partial x^2}-v\frac{\partial u(x,y,t)}{\partial x}. \tag{2.19}$$

Applying Lemma 2.3 and considering (2.18) at point $(x_i,y_j,t_k)$, we have:

$$\begin{aligned}&-\Big(D_1+\frac{v^2h_1^2}{12D_1}\Big)\delta_x^2u_{ij}^k+v\delta_xu_{ij}^k\\&=\Big[1+\frac{h_1^2}{12}\Big(\delta_x^2-\frac{v}{D_1}\delta_x\Big)\Big]\Big[g_{ij}^k-w_{ij}^k+D_2\frac{\partial^2u}{\partial y^2}(x_i,y_j,t_k)\Big]+\big(R_1\big)_{ij}^k,\end{aligned} \tag{2.20}$$

and there exists a positive constant $c_1$ independent of the splitting, such that:

$$\Big|\big(R_1\big)_{ij}^k\Big|\le c_1(h_1^4). \tag{2.21}$$

Similarly, for (2.19), applying the Lemma 2.3 at the point $(x_i,y_j,t_k)$ again, we get:

$$-D_2\delta_y^2u_{ij}^k=\Big[1+\frac{h_2^2}{12}\delta_y^2\Big]\Big[g_{ij}^k-w_{ij}^k+D_1\frac{\partial^2u}{\partial x^2}(x_i,y_j,t_k)-v\frac{\partial u}{\partial x}(x_i,y_j,t_k)\Big]+\big(R_2\big)_{ij}^k, \tag{2.22}$$

and there exists a positive constant $c_2$ independent of the splitting, such that:

$$\Big|\big(R_2\big)_{ij}^k\Big|\le c_2(h_2^4). \tag{2.23}$$

Define $W_{ij}^k=w(x_i,y_j,t_k)$, $(i,j)\in\bar{\omega}$, $0\le k\le K$. Applying the Lemma 2.2, we have:

$$W_{ij}^k = \frac{1}{\Gamma(1-\alpha)} \int_0^{t_k} \frac{\partial u(x_i, y_j, t)}{\partial t} \frac{dt}{(t_k - t)^\alpha}$$
$$= \frac{\tau^{-\alpha}}{\Gamma(2-\alpha)} \Big[ b_0^{(\alpha)} u_{ij}^k - \sum_{m=1}^{k-1} \big( b_{k-m-1}^{(\alpha)} - b_{k-m}^{(\alpha)} \big) u_{ij}^m - b_{k-1}^{(\alpha)} u_{ij}^0 \Big] + (R_3)_{ij}^k, \tag{2.24}$$

and there exists a positive constant $c_3$ independent of the splitting, such that:

$$\left| (R_3)_{ij}^k \right| \le c_3 (\tau^{2-\alpha}). \tag{2.25}$$

Substituting (2.24) into (2.20) and (2.22), adding the two equations together, replacing $w_{ij}^k$ by $W_{ij}^k$, and combing the origan (2.1), we obtain:

$$\begin{aligned}
&- \Big( D_1 + \frac{v^2 h_1^2}{12 D_1} \Big) \delta_x^2 u_{ij}^k + v \delta_x u_{ij}^k - D_2 \delta_y^2 u_{ij}^k \\
&= \Big[ 1 + \frac{h_1^2}{12} \Big( \delta_x^2 - \frac{v}{D_1} \delta_x \Big) \Big] \Big[ g_{ij}^k - W_{ij}^k + D_2 \frac{\partial^2 u}{\partial y^2}(x_i, y_j, t_k) \Big] \\
&\quad + \Big[ 1 + \frac{h_2^2}{12} \delta_y^2 \Big] \Big[ g_{ij}^k - w_{ij}^k + D_1 \frac{\partial^2 u}{\partial x^2}(x_i, y_j, t_k) - v \frac{\partial u}{\partial x}(x_i, y_j, t_k) \Big] + R_{ij}^k \\
&= \Big[ 1 + \frac{h_1^2}{12} \Big( \delta_x^2 - \frac{v}{D_1} \delta_x \Big) + \frac{h_2^2}{12} \delta_y^2 \Big] g_{ij}^k - \Big[ 1 + \frac{h_1^2}{12} \Big( \delta_x^2 - \frac{v}{D_1} \delta_x \Big) + \frac{h_2^2}{12} \delta_y^2 \Big] W_{ij}^k \\
&\quad + D_2 \Big[ \frac{h_1^2}{12} \Big( \delta_x^2 - \frac{v}{D_1} \delta_x \Big) \Big] \frac{\partial^2 u}{\partial y^2}(x_i, y_j, t_k) + D_1 \frac{h_2^2}{12} \delta_y^2 \frac{\partial^2 u}{\partial x^2}(x_i, y_j, t_k) \\
&\quad - v \frac{h_2^2}{12} \delta_y^2 \frac{\partial u}{\partial x}(x_i, y_j, t_k) + R_{ij}^k, \qquad (i, j) \in \omega, \ k = 1, 2, ..., K,
\end{aligned} \tag{2.26}$$

where $R_{i,j}^k = (R_1)_{ij}^k + (R_2)_{ij}^k + (R_3)_{ij}^k$. Besides, from (2.21), (2.23), and (2.25), it is easy to get:

$$|R_{ij}^k| \le c(\tau^{2-\alpha} + h_1^4 + h_2^4), \tag{2.27}$$

where $c = \max\{c_1, \ c_2, \ c_3\}$.

In (2.26), the first-order derivative term is approximated by the first-order central difference formula:

$$\frac{\partial u}{\partial x}(x_i, y_j, t_k) = \frac{u_{i+1,j}^k - u_{i-1,j}^k}{2h} + \mathcal{O}(h_1^2). \tag{2.28}$$

The second-order derivative terms are approximated by the second-order central difference formulas:

$$\frac{\partial^2 u}{\partial x^2}(x_i, y_j, t_k) = \frac{u_{i+1,j}^k - 2u_{ij}^k + u_{i-1,j}^k}{h^2} + \mathcal{O}(h_1^2), \tag{2.29}$$

and

$$\frac{\partial^2 u}{\partial y^2}(x_i, y_j, t_k) = \frac{u_{i,j+1}^k - 2u_{ij}^k + u_{i,j-1}^k}{h^2} + \mathcal{O}(h_2^2). \tag{2.30}$$

Using the notations defined in (2.4), (2.26) can be written to:

$$
\begin{aligned}
&-\Big(D_1+\frac{v^2h_1^2}{12D_1}\Big)\delta_x^2u_{ij}^k+v\delta_xu_{ij}^k-D_2\delta_y^2u_{ij}^k\\
&=\Big[1+\frac{h_1^2}{12}\Big(\delta_x^2-\frac{v}{D_1}\delta_x\Big)+\frac{h_2^2}{12}\delta_y^2\Big]g_{ij}^k-\Big[1+\frac{h_1^2}{12}\Big(\delta_x^2-\frac{v}{D_1}\delta_x\Big)+\frac{h_2^2}{12}\delta_y^2\Big]W_{ij}^k\\
&\quad+D_2\Big[\frac{h_1^2}{12}\Big(\delta_x^2-\frac{v}{D_1}\delta_x\Big)\Big]\delta_y^2u_{ij}^k+D_1\frac{h_2^2}{12}\delta_y^2\delta_x^2u_{ij}^k-v\frac{h_2^2}{12}\delta_y^2\delta_xu_{ij}^k+\hat{R}_{ij}^k,
\end{aligned}
\tag{2.31}
$$

where $(i,\,j)\in\omega,\ k=1,2,...,K$.

**Lemma 2.4** *The local truncation error in* (2.31) *is:*

$$
\Big|\hat{R}_{ij}^k\Big|=\mathscr{O}(\tau^{2-\alpha}+h_1^4+h_2^4),\qquad (i,\,j)\in\omega,\ 1\le k\le K.
\tag{2.32}
$$

***Proof*** Plugging the central difference approximation formulas (2.28)–(2.30) for the first-order and second-order derivatives and the corresponding notations (2.4) back into (2.26), we obtain:

$$
\begin{aligned}
&-\Big(D_1+\frac{v^2h_1^2}{12D_1}\Big)\delta_x^2u_{ij}^k+v\delta_xu_{ij}^k-D_2\delta_y^2u_{ij}^k\\
&=\Big[1+\frac{h_1^2}{12}\Big(\delta_x^2-\frac{v}{D_1}\delta_x\Big)+\frac{h_2^2}{12}\delta_y^2\Big]g_{ij}^k-\Big[1+\frac{h_1^2}{12}\Big(\delta_x^2-\frac{v}{D_1}\delta_x\Big)+\frac{h_2^2}{12}\delta_y^2\Big]W_{ij}^k\\
&\quad+D_2\Big[\frac{h_1^2}{12}\Big(\delta_x^2-\frac{v}{D_1}\delta_x\Big)\Big]\Big[\delta_y^2u_{ij}^k+\mathscr{O}(h_2^2)\Big]+D_1\frac{h_2^2}{12}\delta_y^2\Big[\delta_x^2u_{ij}^k+\mathscr{O}(h_1^2)\Big]\\
&\quad-v\frac{h_2^2}{12}\delta_y^2\Big[\delta_xu_{ij}^k+\mathscr{O}(h_1^2)\Big]+R_{ij}^k\\
&=\Big[1+\frac{h_1^2}{12}\Big(\delta_x^2-\frac{v}{D_1}\delta_x\Big)+\frac{h_2^2}{12}\delta_y^2\Big]g_{ij}^k-\Big[1+\frac{h_1^2}{12}\Big(\delta_x^2-\frac{v}{D_1}\delta_x\Big)+\frac{h_2^2}{12}\delta_y^2\Big]W_{ij}^k\\
&\quad+D_2\Big[\frac{h_1^2}{12}\Big(\delta_x^2-\frac{v}{D_1}\delta_x\Big)\Big]\delta_y^2u_{ij}^k+D_1\frac{h_2^2}{12}\delta_y^2\delta_x^2u_{ij}^k-v\frac{h_2^2}{12}\delta_y^2\delta_xu_{ij}^k\\
&\quad+D_2\Big[\frac{h_1^2}{12}\Big(\delta_x^2-\frac{v}{D_x}\delta_x\Big)\Big]\mathscr{O}(h_2^2)+D_1\frac{h_2^2}{12}\mathscr{O}(h_1^2)-v\frac{h_2^2}{12}\delta_y^2\mathscr{O}(h_1^2)+R_{ij}^k\\
&=\Big[1+\frac{h_1^2}{12}\Big(\delta_x^2-\frac{v}{D_1}\delta_x\Big)+\frac{h_2^2}{12}\delta_y^2\Big]g_{ij}^k-\Big[1+\frac{h_1^2}{12}\Big(\delta_x^2-\frac{v}{D_1}\delta_x\Big)+\frac{h_2^2}{12}\delta_y^2\Big]W_{ij}^k\\
&\quad+D_2\Big[\frac{h_1^2}{12}\Big(\delta_x^2-\frac{v}{D_1}\delta_x\Big)\Big]\delta_y^2u_{ij}^k+D_1\frac{h_2^2}{12}\delta_y^2\delta_x^2u_{ij}^k-v\frac{h_2^2}{12}\delta_y^2\delta_xu_{ij}^k\\
&\quad+\mathscr{O}(h_1^2h_2^2)+\mathscr{O}(h_1^2h_1^2)-\mathscr{O}(h_1^2h_1^2)+R_{ij}^k,\quad (i,\,j)\in\omega,\ k=1,2,...,K.
\end{aligned}
\tag{2.33}
$$

From the triangle inequality $ab\le\frac{a^2+b^2}{2}$, it is apparent that $\mathscr{O}(h_1^2h_2^2)$ and $\mathscr{O}(h_1^4+h_2^4)$ are equivalent. In (2.33), let:

$$
\mathscr{O}(h_1^2h_2^2)+\mathscr{O}(h_1^2h_1^2)-\mathscr{O}(h_1^2h_1^2)+R_{ij}^k=\hat{R}_{ij}^k,
\tag{2.34}
$$

Combining the definition of $R_{ij}^k$ in (2.27), it gives:

$$
\Big|\hat{R}_{ij}^k\Big|\le C_0(\tau^{2-\alpha}+h_1^4+h_2^4),\qquad (i,\,j)\in\omega,\ 1\le k\le K,
\tag{2.35}
$$

where $C_0$ is a constant different from the $c$ derived in (2.27) but independent of the splitting.

As a result, we have:

$$\left|\hat{R}_{ij}^{k}\right| = \mathscr{O}(\tau^{2-\alpha} + h_1^4 + h_2^4), \qquad (i, j) \in \omega,\ 1 \le k \le K. \tag{2.36}$$

This completes the proof. □

Let:

$$\gamma_x = \frac{D_1}{12h_1^2}, \quad \gamma_y = \frac{D_2}{12h_2^2}, \quad \gamma_v = \frac{v}{2h_1}, \quad \nu = \frac{vh_1}{24D_1},$$
$$\mu = \frac{\tau^{-\alpha}}{\Gamma(2-\alpha)}, \quad \zeta = \frac{\left(\frac{h_1^2 D_2 v}{12D_1} + \frac{vh_2^2}{12}\right)}{2h_1h_2^2}, \quad \gamma = \frac{\left(D_1 + \frac{(vh_1)^2}{12D_1}\right)}{h_1^2}.$$

And define:

$$\begin{cases} a_1 = 2\gamma - 4\gamma_x + 20\gamma_y + \dfrac{2}{3}\mu, \\ a_2 = -\gamma + \gamma_v + 2(\gamma_x + \gamma_y) - 2\zeta + \left(\dfrac{1}{12} - \nu\right)\mu, \\ a_3 = -\gamma - \gamma_v + 2(\gamma_x + \gamma_y) + 2\zeta + \left(\dfrac{1}{12} + \nu\right)\mu, \\ a_4 = 2\gamma_x - 10\gamma_y + \dfrac{1}{12}\mu, \\ a_5 = -(\gamma_x + \gamma_y) + \zeta, \\ a_6 = -(\gamma_x + \gamma_y) - \zeta, \end{cases} \tag{2.37}$$

$$\begin{cases} b_1 = \dfrac{2}{3}, \\ b_2 = \dfrac{1}{12} - \nu, \\ b_3 = \dfrac{1}{12} + \nu, \\ b_4 = \dfrac{1}{12}. \end{cases} \tag{2.38}$$

Then, for $\forall (i, j) \in \omega,\ k = 1, 2, ..., K$, (2.31) becomes:

$$\begin{aligned} &a_1 u_{ij}^k + a_2 u_{i+1,j}^k + a_3 u_{i-1,j}^k + a_4 u_{i,j+1}^k + a_4 u_{i,j-1}^k \\ &\quad + a_5 u_{i+1,j+1}^k + a_6 u_{i-1,j+1}^k + a_5 u_{i+1,j-1}^k + a_6 u_{i-1,j-1}^k s \\ &= b_1 g_{ij}^k + b_2 g_{i+1,j}^k + b_3 g_{i-1,j}^k + b_4 g_{i,j+1}^k + b_4 g_{i,j-1}^k \\ &\quad + b_1\mu \sum_{m=1}^{k-1} \left[b_{k-m-1}^{(\alpha)} - b_{k-m}^{(\alpha)}\right] u_{ij}^m + b_2\mu \sum_{m=1}^{k-1} \left[b_{k-m-1}^{(\alpha)} - b_{k-m}^{(\alpha)}\right] u_{i+1,j}^m \\ &\quad + b_3\mu \sum_{m=1}^{k-1} \left[b_{k-m-1}^{(\alpha)} - b_{k-m}^{(\alpha)}\right] u_{i-1,j}^m + b_4\mu \sum_{m=1}^{k-1} \left[b_{k-m-1}^{(\alpha)} - b_{k-m}^{(\alpha)}\right] u_{i,j+1}^m \\ &\quad + b_4\mu \sum_{m=1}^{k-1} \left[b_{k-m-1}^{(\alpha)} - b_{k-m}^{(\alpha)}\right] u_{i,j-1}^m + b_1\mu b_{k-1}^{(\alpha)} u_{ij}^0 + b_2\mu b_{k-1}^{(\alpha)} u_{i+1,j}^0 \\ &\quad + b_3\mu b_{k-1}^{(\alpha)} u_{i-1,j}^0 + b_4\mu b_{k-1}^{(\alpha)} u_{i,j+1}^0 + b_4\mu b_{k-1}^{(\alpha)} u_{i,j-1}^0 + \hat{R}_{ij}^k. \end{aligned} \tag{2.39}$$

Noting the initial value and boundary-value conditions (2.2)–(2.3), we have:

$$\begin{cases} u_{ij}^0 = \varphi(x_i, y_j), & \forall\ (i,j) \in \omega, \\ u_{0,y}^k(0,y) = \psi_1(y,t_k), \quad u_{l_1,y}^k(l_1,y) = \psi_2(y,t_k), & \forall\ y \in (0,l_2),\ 1 \le k \le K, \\ u_{x,0}^k(x,0) = \phi_1(x,t_k), \quad u_{x,l_2}^k(x,l_2) = \phi_2(x,t_k), & \forall\ x \in (0,l_1),\ 1 \le k \le K. \end{cases} \tag{2.40}$$

Accordingly, we have:

$$\begin{cases} \psi_1(0,t_k) = \phi_1(0,t_k), \quad \phi_1(l_1,t_k) = \psi_2(0,t_k), \\ \psi_2(l_2,t_k) = \phi_2(l_1,t_k), \quad \phi_2(0,t_k) = \psi_1(l_2,t_k), \end{cases} \quad 1 \le k \le K. \tag{2.41}$$

Omitting the small item $\hat{R}_{ij}^k$ in (2.39) as well as replacing $u_{ij}^k$ by its approximation solution $U_{ij}^k$, we derive the CFDS of IBVP with fourth order in spatial and $(2-\alpha)$-order in temporal:

$$\begin{aligned} &a_1 U_{ij}^k + a_2 U_{i+1,j}^k + a_3 U_{i-1,j}^k + a_4 U_{i,j+1}^k + a_4 U_{i,j-1}^k \\ &\quad + a_5 U_{i+1,j+1}^k + a_6 U_{i-1,j+1}^k + a_5 U_{i+1,j-1}^k + a_6 U_{i-1,j-1}^k \\ &= b_1 g_{ij}^k + b_2 g_{i+1,j}^k + b_3 g_{i-1,j}^k + b_4 g_{i,j+1}^k + b_4 g_{i,j-1}^k \\ &\quad + b_1\mu \sum_{m=1}^{k-1} \left[b_{k-m-1}^{(\alpha)} - b_{k-m}^{(\alpha)}\right] U_{ij}^m + b_2\mu \sum_{m=1}^{k-1} \left[b_{k-m-1}^{(\alpha)} - b_{k-m}^{(\alpha)}\right] U_{i+1,j}^m \\ &\quad + b_3\mu \sum_{m=1}^{k-1} \left[b_{k-m-1}^{(\alpha)} - b_{k-m}^{(\alpha)}\right] U_{i-1,j}^m + b_4\mu \sum_{m=1}^{k-1} \left[b_{k-m-1}^{(\alpha)} - b_{k-m}^{(\alpha)}\right] U_{i,j+1}^m \\ &\quad + b_4\mu \sum_{m=1}^{k-1} \left[b_{k-m-1}^{(\alpha)} - b_{k-m}^{(\alpha)}\right] U_{i,j-1}^m + b_1\mu b_{k-1}^{(\alpha)} U_{ij}^0 + b_2\mu b_{k-1}^{(\alpha)} U_{i+1,j}^0 \\ &\quad + b_3\mu b_{k-1}^{(\alpha)} U_{i-1,j}^0 + b_4\mu b_{k-1}^{(\alpha)} U_{i,j+1}^0 + b_4\mu b_{k-1}^{(\alpha)} U_{i,j-1}^0, \quad (i,j) \in \omega,\ k = 1,2,\ldots,K, \end{aligned} \tag{2.42}$$

$$u_{ij}^0 = \varphi(x_i, y_j), \qquad (i,j) \in \omega, \tag{2.43}$$

$$\begin{aligned} &u_{0,y}^k(0,y) = \psi_1(y,t_k), \quad u_{l_1,y}^k(l_1,y) = \psi_2(y,t_k), \qquad y \in (0,l_2),\ 1 \le k \le K, \\ &u_{x,0}^k(x,0) = \phi_1(x,t_k), \quad u_{x,l_2}^k(x,l_2) = \phi_2(x,t_k), \qquad x \in (0,l_1),\ 1 \le k \le K, \end{aligned} \tag{2.44}$$

$$\begin{aligned} &\psi_1(0,t_k) = \phi_1(0,t_k), \quad \phi_1(l_1,t_k) = \psi_2(0,t_k), \\ &\psi_2(l_2,t_k) = \phi_2(l_1,t_k), \quad \phi_2(0,t_k) = \psi_1(l_2,t_k), \qquad 1 \le k \le K. \end{aligned} \tag{2.45}$$

## 3 Matrix form of the numerical scheme

Suppose that:

$$\mathbf{U}_j^k = \begin{bmatrix} U_{1j}^k \\ U_{2j}^k \\ \vdots \\ U_{N_1-1,j}^k \end{bmatrix}, \quad 0 \le j \le N_2 - 1, \qquad \mathbf{U}^k = \begin{bmatrix} \mathbf{U}_1^k \\ \mathbf{U}_2^k \\ \vdots \\ \mathbf{U}_{N_2-1}^k \end{bmatrix}.$$

Similarly, we can define $\mathbf{g}^k$ by referring to the definition of $\mathbf{U}^k$. Then, we consider scheme (2.42) on each spatial grid points, and the original problem is transformed into solving such a linear algebraic equations at each time layer:

$$\mathbf{A}\mathbf{U}^k = \mathbf{B}\mathbf{g}^k + \mu \sum_{m=1}^{k-1} (b_{k-m-1}^{(\alpha)} - b_{k-m}^{(\alpha)})\mathbf{B}\mathbf{U}^m + \mu b_{k-1}^{(\alpha)} \mathbf{B}\mathbf{U}^0, \tag{3.1}$$

where $k \geq 2$.

when $k = 1$, (2.10) leads to:

$$ {}_0^C D_t^\alpha u(x, y, t)\Big|_{t=t_1} \approx \frac{\tau^{-\alpha}}{\Gamma(2-\alpha)} \Big[ u(x, y, t_1) - u(x, y, t_0) \Big].$$

Therefore, the linear algebraic equations needed to be solved becomes:

$$\mathbf{A}\mathbf{U}^1 = \mathbf{B}\mathbf{g}^1 + \mu \mathbf{B}\mathbf{U}^0. \tag{3.2}$$

We will give matrix $\mathbf{A}$, matrix $\mathbf{B}$, and vector $\mathbf{g}$ in (3.1)–(3.2) and their constituent elements. The elements defined by (2.37) can be assembled into tri-diagonal matrix with dimensions of $(N_1 - 1) \times (N_2 - 1)$:

$$\mathbf{A_1} = \begin{bmatrix} a_1 & a_2 & & & \\ a_3 & a_1 & a_2 & & \\ & \ddots & \ddots & \ddots & \\ & & a_3 & a_1 & a_2 \\ & & & a_3 & a_1 \end{bmatrix}, \quad \mathbf{A_2} = \begin{bmatrix} a_4 & a_5 & & & \\ a_6 & a_4 & a_5 & & \\ & \ddots & \ddots & \ddots & \\ & & a_6 & a_4 & a_5 \\ & & & a_6 & a_4 \end{bmatrix}.$$

Similarly, the elements defined by (2.38) can also be assembled into two matrixes: one tri-diagonal matrix with dimension of $(N_1 - 1) \times (N_2 - 1)$ and another matrix with a main diagonal only but same dimension:

$$\mathbf{B_1} = \begin{bmatrix} b_1 & b_2 & & & \\ b_3 & b_1 & b_2 & & \\ & \ddots & \ddots & \ddots & \\ & & b_3 & b_1 & b_2 \\ & & & b_3 & b_1 \end{bmatrix}, \quad \mathbf{B_2} = \begin{bmatrix} b_4 & & & & \\ & b_4 & & & \\ & & \ddots & & \\ & & & b_4 & \\ & & & & b_4 \end{bmatrix}.$$

With the above work, we can easily give the matrix $\mathbf{A}$, matrix $\mathbf{B}$, and vector $\mathbf{g}$:

$$\mathbf{A} = \begin{bmatrix} \mathbf{A}_1 & \mathbf{A}_2 & & & \\ \mathbf{A}_2 & \mathbf{A}_1 & \mathbf{A}_2 & & \\ & \ddots & \ddots & \ddots & \\ & & \mathbf{A}_2 & \mathbf{A}_1 & \mathbf{A}_2 \\ & & & \mathbf{A}_2 & \mathbf{A}_1 \end{bmatrix}, \quad \mathbf{B} = \begin{bmatrix} \mathbf{B}_1 & \mathbf{B}_2 & & & \\ \mathbf{B}_2 & \mathbf{B}_1 & \mathbf{B}_2 & & \\ & \ddots & \ddots & \ddots & \\ & & \mathbf{B}_2 & \mathbf{B}_1 & \mathbf{B}_2 \\ & & & \mathbf{B}_2 & \mathbf{B}_1 \end{bmatrix},$$

$$\mathbf{g} = \begin{bmatrix} \left[1 + \frac{h_1^2}{12}\left(\delta_x^2 - \frac{v}{D_1}\delta_x\right) + \frac{h_2^2}{12}\delta_y^2\right]\mathbf{g_1} + \mathbf{A_2 U_0} \\ \left[1 + \frac{h_1^2}{12}\left(\delta_x^2 - \frac{v}{D_1}\delta_x\right) + \frac{h_2^2}{12}\delta_y^2\right]\mathbf{g_2} \\ \vdots \\ \left[1 + \frac{h_1^2}{12}\left(\delta_x^2 - \frac{v}{D_1}\delta_x\right) + \frac{h_2^2}{12}\delta_y^2\right]\mathbf{g_{N_1-2}} \\ \left[1 + \frac{h_1^2}{12}\left(\delta_x^2 - \frac{v}{D_1}\delta_x\right) + \frac{h_2^2}{12}\delta_y^2\right]\mathbf{g_{N_1-1}} + \mathbf{A_2 U_{N_2}} \end{bmatrix}.$$

It follows that matrix $\mathbf{A}$ is a nine-diagonal matrix with dimension of $(N_1-1)\cdot(N_2-1)\times(N_1-1)\cdot(N_2-1)$, and matrix $\mathbf{A}_1$ and matrix $\mathbf{A}_2$ are both tri-diagonal matrixes with dimension of $(N_1-1)\times(N_2-1)$. Matrix $\mathbf{A}$ is also referred to as block tri-diagonal matrix. In addition, matrix $\mathbf{B}$ is a five-diagonal matrix with dimension of $(N_1-1)\cdot(N_2-1)\times(N_1-1)\cdot(N_2-1)$. In its constituent elements, one is a tri-diagonal matrix $\mathbf{B}_1$ with dimension of $(N_1-1)\times(N_2-1)$; another is a main diagonal matrix $\mathbf{B}_2$ with dimension of $(N_1-1)\times(N_2-1)$. $\mathbf{g}$ is a column vector with dimension of $(N_1-1)\cdot(N_2-1)\times 1$.

## 4 Unique solvability

**Definition 4.1** (Fatoorehchi and Abolghasemi 2014) (Gershgorin disk) Let $\mathbf{C} = (c_{ij})_{n\times n}$ for $c_{ij} \in \mathbb{C}$, $(i, j = 1, 2, ..., n)$ be a complex $n \times n$ matrix and let $r_i = \sum_{j\neq i}^{n} |c_{ij}|$, $(i = 1, 2, ..., n)$ be the sum of absolute values of the non-diagonal entries in the $i^{th}$ row; the set:

$$D_i = \{\, z \mid |z - c_{ii}| \leq r_i,\ z \in \mathbb{C}\},$$

is a closed disc (Gershgorin disk) with center $c_{ii}$ and radius $r_i$ on the complex plane.

**Lemma 4.1** (Fatoorehchi and Abolghasemi 2014 (Gershgorin circle theorem) *Each eigenvalue $\lambda$ of $\mathbf{C}$ must lie within one of the Gershgorin disks, i.e., $|\lambda - c_{ii}| \leq r_i (i = 1, 2, ..., n)$. That is to say, all eigenvalues of $\mathbf{C}$ are in the union of n discs on the complex plane.*

***Proof*** The proof has been given in the work of (Gershgorin 1931; Feingold et al. 1962); we omit it here for brevity. □

**Theorem 4.1** *The coefficient matrix $\mathbf{A}$ in (3.1) and (3.2) is invertible.*

***Proof*** First, according to the definition of $a_i$ $(1 \leq i \leq 6)$ in Eq. (2.37), it can be easily to see that $a_1 > 0$ for any spatial step sizes $h_1, h_2$ and any temporal step sizes $\tau$ when both diffusion coefficients $D_1, D_2$ and convect coefficient $v$ are fixed. At the same time, it is evident that $a_i < 0$ $(2 \leq i \leq 6)$ by a routine computation.

The next step in the proof is to find the range of eigenvalues of matrix $\mathbf{A}$. Combining the symmetry of $\mathbf{A}$ between the elements above the secondary diagonal and below the secondary diagonal, according to Definition 4.1 and Lemma 4.1, it follows that each eigenvalue $\lambda$ of $\mathbf{A}$ is lain within in one of the following discs; it yields:

$$|\lambda - a_1| \leq |a_3| + |a_4| + |a_5|,$$
$$|\lambda - a_1| \leq |a_3| + |a_2| + |a_6| + |a_4| + |a_5|,$$
$$|\lambda - a_1| \leq |a_3| + |a_6| + |a_4|,$$

$$
\begin{aligned}
&|\lambda - a_1| \le |a_4| + |a_4| + |a_2| + |a_4| + |a_5|,\\
&|\lambda - a_1| \le |a_6| + |a_4| + |a_5| + |a_3| + |a_2| + |a_6| + |a_4| + |a_5|,\\
&|\lambda - a_1| \le |a_6| + |a_4| + |a_3| + |a_6| + |a_4|.
\end{aligned} \tag{4.1}
$$

In other words, let $b = |a_6| + |a_4| + |a_5| + |a_3| + |a_2| + |a_6| + |a_4| + |a_5|$; each eigenvalue $\lambda$ of $\mathbf{A}$ is satisfied with:

$$
a_1 - b \le \lambda \le a_1 + b. \tag{4.2}
$$

At last, it is easy to prove $a_1 + b > 0$ in (4.2). By means of the definition of $\mu$, we have:

$$
\begin{aligned}
a_1 - b &= a_1 - \Big(|a_6| + |a_4| + |a_5| + |a_3| + |a_2| + |a_6| + |a_4| + |a_5|\Big)\\
&= \Big[2\gamma + \frac{2D_y}{h_2^2} - 4(\gamma_x + \gamma_y) + \frac{2}{3}\mu\Big] - \Big[2\gamma - 4(\gamma_x + \gamma_y) - \frac{1}{3}\mu + \frac{2D_y}{h_2^2}\Big]\\
&= \frac{2}{3}\mu + \frac{1}{3}\mu\\
&= \mu > 0.
\end{aligned} \tag{4.3}
$$

In conclusion, all eigenvalues of the matrix $\mathbf{A}$ are not 0 for any spatial step sizes $h_1, h_2$ and any temporal step sizes $\tau$. Thus, we arrive at the conclusion that matrix $\mathbf{A}$ is invertible. □

**Theorem 4.2** *The CFDS (2.42) has a unique solution.*

***Proof*** To get the numerical solution of original problem (2.1) on each time layer $t_k = k\tau$, we need to solve a linear algebraic equations. Namely, when $k = 1$, we need to solve (3.2). Otherwise, when $k = 2, 3, ..., K$, we need to solve (3.1). In addition, we recognize that matrix $\mathbf{A}$ is invertible, it follows that the CFDS (2.42) has a unique solution. □

## 5 Stability analysis

**Theorem 5.1** *Let $\{v_{ij}^k | (i, j) \in \omega, 1 \le k \le K\}$ be the solution of CFDS:*

$$
\begin{aligned}
&a_1 v_{ij}^k + a_2 v_{i+1,j}^k + a_3 v_{i-1,j}^k + a_4 v_{i,j+1}^k + a_4 v_{i,j-1}^k\\
&\quad + a_5 v_{i+1,j+1}^k + a_6 v_{i-1,j+1}^k + a_5 v_{i+1,j-1}^k + a_6 v_{i-1,j-1}^k\\
&= b_1\mu \sum_{m=1}^{k-1} \big[b_{k-m-1}^{(\alpha)} - b_{k-m}^{(\alpha)}\big] v_{ij}^m + b_2\mu \sum_{m=1}^{k-1} \big[b_{k-m-1}^{(\alpha)} - b_{k-m}^{(\alpha)}\big] v_{i+1,j}^m\\
&\quad + b_3\mu \sum_{m=1}^{k-1} \big[b_{k-m-1}^{(\alpha)} - b_{k-m}^{(\alpha)}\big] v_{i-1,j}^m + b_4\mu \sum_{m=1}^{k-1} \big[b_{k-m-1}^{(\alpha)} - b_{k-m}^{(\alpha)}\big] v_{i,j+1}^m\\
&\quad + b_4\mu \sum_{m=1}^{k-1} \big[b_{k-m-1}^{(\alpha)} - b_{k-m}^{(\alpha)}\big] v_{i,j-1}^m + b_1\mu b_{k-1}^{(\alpha)} v_{ij}^0 + b_2\mu b_{k-1}^{(\alpha)} v_{i+1,j}^0 + b_3\mu b_{k-1}^{(\alpha)} v_{i-1,j}^0\\
&\quad + b_4\mu b_{k-1}^{(\alpha)} v_{i,j+1}^0 + b_4\mu b_{k-1}^{(\alpha)} v_{i,j-1}^0 + f_{ij}^k, \qquad (i, j) \in \omega,\ 1 \le k \le K,
\end{aligned} \tag{5.1}
$$

$$
v_{ij}^0 = \varphi(x_i, y_j), \qquad (i, j) \in \omega, \tag{5.2}
$$

$$
v_{ij}^k = 0, \qquad (i, j) \in \partial\omega,\ 1 \le k \le K, \tag{5.3}
$$

*then there exists certain a positive constant $C_1$ independent of the splitting, such that:*

$$\|v^k\|_\infty \le C_1\left(\|v^0\|_\infty + t_k^\alpha \Gamma(1-\alpha)\max_{1\le n\le k}\|f^n\|_\infty\right), \qquad 1\le k\le K, \tag{5.4}$$

*where $f_{ij}^k$ represents a small perturbation of the source term at the right end, and:*

$$\|v^k\|_\infty = \max_{(i,j)\in\bar{\omega}}|v_{ij}^k|, \qquad \|f^n\|_\infty = \max_{(i,j)\in\omega}|f_{ij}^n|.$$

***Proof*** (5.1) can be written to the following form equivalently:

$$\begin{aligned}
a_1 v_{ij}^k = &-\Big[a_2 v_{i+1,j}^k + a_3 v_{i-1,j}^k + a_4 v_{i,j+1}^k + a_4 v_{i,j-1}^k \\
&+ a_5 v_{i+1,j+1}^k + a_6 v_{i-1,j+1}^k + a_5 v_{i+1,j-1}^k + a_6 v_{i-1,j-1}^k\Big] \\
&+ b_1\mu\sum_{m=1}^{k-1}[b_{k-m-1}^{(\alpha)} - b_{k-m}^{(\alpha)}]v_{ij}^m + b_2\mu\sum_{m=1}^{k-1}[b_{k-m-1}^{(\alpha)} - b_{k-m}^{(\alpha)}]v_{i+1,j}^m \\
&+ b_3\mu\sum_{m=1}^{k-1}[b_{k-m-1}^{(\alpha)} - b_{k-m}^{(\alpha)}]v_{i-1,j}^m + b_4\mu\sum_{m=1}^{k-1}[b_{k-m-1}^{(\alpha)} - b_{k-m}^{(\alpha)}]v_{i,j+1}^m \\
&+ b_4\mu\sum_{m=1}^{k-1}[b_{k-m-1}^{(\alpha)} - b_{k-m}^{(\alpha)}]v_{i,j-1}^m + b_1\mu b_{k-1}^{(\alpha)}v_{ij}^0 + b_2\mu b_{k-1}^{(\alpha)}v_{i+1,j}^0 + b_3\mu b_{k-1}^{(\alpha)}v_{i-1,j}^0 \\
&+ b_4\mu b_{k-1}^{(\alpha)}v_{i,j+1}^0 + b_4\mu b_{k-1}^{(\alpha)}v_{i,j-1}^0 + f_{ij}^k, \qquad (i,j)\in\omega,\ 1\le k\le K.
\end{aligned} \tag{5.5}$$

Define $\|v^k\|_\infty = |v_{i_n,j_n}^k|$, where $i_n \in \{1,2,...,N_1-1\}$, $j_n \in \{1,2,...,N_2-1\}$. For $\forall\,(i,j)\in\omega$, $1\le k\le K$, taking absolute value to both sides, we have:

$$\begin{aligned}
\left|a_1 v_{ij}^k\right| = \Big| &-\Big[a_2 v_{i+1,j}^k + a_3 v_{i-1,j}^k + a_4 v_{i,j+1}^k + a_4 v_{i,j-1}^k \\
&+ a_5 v_{i+1,j+1}^k + a_6 v_{i-1,j+1}^k + a_5 v_{i+1,j-1}^k + a_6 v_{i-1,j-1}^k\Big] \\
&+ b_1\mu\sum_{m=1}^{k-1}[b_{k-m-1}^{(\alpha)} - b_{k-m}^{(\alpha)}]v_{ij}^m + b_2\mu\sum_{m=1}^{k-1}[b_{k-m-1}^{(\alpha)} - b_{k-m}^{(\alpha)}]v_{i+1,j}^m \\
&+ b_3\mu\sum_{m=1}^{k-1}[b_{k-m-1}^{(\alpha)} - b_{k-m}^{(\alpha)}]v_{i-1,j}^m + b_4\mu\sum_{m=1}^{k-1}[b_{k-m-1}^{(\alpha)} - b_{k-m}^{(\alpha)}]v_{i,j+1}^m \\
&+ b_4\mu\sum_{m=1}^{k-1}[b_{k-m-1}^{(\alpha)} - b_{k-m}^{(\alpha)}]v_{i,j-1}^m + b_1\mu b_{k-1}^{(\alpha)}v_{ij}^0 + b_2\mu b_{k-1}^{(\alpha)}v_{i+1,j}^0 + b_3\mu b_{k-1}^{(\alpha)}v_{i-1,j}^0 \\
&+ b_4\mu b_{k-1}^{(\alpha)}v_{i,j+1}^0 + b_4\mu b_{k-1}^{(\alpha)}v_{i,j-1}^0 + f_{ij}^k\Big|.
\end{aligned} \tag{5.6}$$

Using triangle inequality, it derives:

$$\begin{aligned}
|a_1|\|v^k\|_\infty &\le |a_2+a_3+a_4+a_4+a_5+a_6+a_5+a_6|\|v^k\|_\infty \\
&\quad + \left|\mu\sum_{m=1}^{k-1}\left[b_{k-m-1}^{(\alpha)} - b_{k-m}^{(\alpha)}\right](b_1+b_2+b_3+b_4+b_4)\right|\|v^m\|_\infty \\
&\quad + \left|\mu b_{k-1}^{(\alpha)}(b_1+b_2+b_3+b_4+b_4)\right|\|v^0\|_\infty + \|f^k\|_\infty \\
&\le \Big[|a_2|+|a_3|+|a_4|+|a_4|+|a_5|+|a_6|+|a_5|+|a_6|\Big]\|v^k\|_\infty
\end{aligned}$$

$$+\mu\sum_{m=1}^{k-1}\left[b_{k-m-1}^{(\alpha)}-b_{k-m}^{(\alpha)}\right]\Big[|b_1|+|b_2|+|b_3|+|b_4|+|b_4|\Big]\|v^m\|_\infty$$
$$+\mu b_{k-1}^{(\alpha)}\Big[|b_1|+|b_2|+|b_3|+|b_4|+|b_4|\Big]\|v^0\|_\infty+\|f^k\|_\infty. \tag{5.7}$$

Therefore, we get:

$$\Big\{|a_1|-\Big[|a_2|+|a_3|+|a_4|+|a_4|+|a_5|+|a_6|+|a_5|+|a_6|\Big]\Big\}\|v^k\|_\infty$$
$$\le\mu\sum_{m=1}^{k-1}\left[b_{k-m-1}^{(\alpha)}-b_{k-m}^{(\alpha)}\right]\Big[|b_1|+|b_2|+|b_3|+|b_4|+|b_4|\Big]\|v^m\|_\infty$$
$$+\mu b_{k-1}^{(\alpha)}\Big[|b_1|+|b_2|+|b_3|+|b_4|+|b_4|\Big]\|v^0\|_\infty+\|f^k\|_\infty. \tag{5.8}$$

Noting that $|a_1|-\Big[|a_2|+|a_3|+|a_4|+|a_4|+|a_5|+|a_6|+|a_5|+|a_6|\Big]=\mu>0$ in (4.3); let $C_1=|b_1+b_2+b_3+b_4+b_4|$, (5.8) becomes:

$$\mu\|v^k\|_\infty\le\mu C_1\sum_{m=1}^{k-1}\left[b_{n-m-1}^{(\alpha)}-b_{n-m}^{(\alpha)}\right]\|v^m\|_\infty+\mu C_1 b_{k-1}^{(\alpha)}\|v^0\|_\infty+\|f^k\|_\infty. \tag{5.9}$$

Thus, we have:

$$\|v^k\|_\infty\le C_1\sum_{m=1}^{k-1}\left[b_{k-m-1}^{(\alpha)}-b_{k-m}^{(\alpha)}\right]\|v^m\|_\infty+C_1 b_{k-1}^{(\alpha)}\left\{\|v^0\|_\infty+\frac{1}{\mu C_1 b_{k-1}^{(\alpha)}}\|f^k\|_\infty\right\},$$
$$=C_1\left\{\sum_{m=1}^{k-1}\left[b_{k-m-1}^{(\alpha)}-b_{k-m}^{(\alpha)}\right]\|v^m\|_\infty+b_{k-1}^{(\alpha)}\left[\|v^0\|_\infty+\frac{1}{\mu C_1 b_{k-1}^{(\alpha)}}\|f^k\|_\infty\right]\right\}, \tag{5.10}$$

Taking Lemma 2.1 into consideration, we get:

$$\frac{1}{\mu b_{n-1}^{(\alpha)}}\le\frac{\tau^\alpha\Gamma(2-\alpha)}{(1-\alpha)n^{-\alpha}}=(k\tau)^\alpha\Gamma(1-\alpha). \tag{5.11}$$

By submitting (5.11) into (5.10), we obtain:

$$\|v^k\|_\infty\le C_1\left\{\sum_{m=1}^{k-1}\left[b_{k-m-1}^{(\alpha)}-b_{k-m}^{(\alpha)}\right]\|v^m\|_\infty+b_{k-1}^{(\alpha)}\left[\|v^0\|_\infty+\frac{1}{C_1}t_k^\alpha\Gamma(1-\alpha)\|f^k\|_\infty\right]\right\}. \tag{5.12}$$

Due to $\dfrac{1}{C_1}<1$, (5.12) becomes:

$$\|v^k\|_\infty\le C_1\left\{\sum_{m=1}^{k-1}\left[b_{k-m-1}^{(\alpha)}-b_{k-m}^{(\alpha)}\right]\|v^m\|_\infty+b_{k-1}^{(\alpha)}\left[\|v^0\|_\infty+t_k^\alpha\Gamma(1-\alpha)\|f^k\|_\infty\right]\right\}. \tag{5.13}$$

Next, using inequality (5.13), we will prove Theorem 5.1 by mathematical inductive method.

(1) Considering (5.13) with $k = 1$, we find that:

$$\|v^1\|_\infty \le C_1 \left(\|v^0\|_\infty + t_1^\alpha \Gamma(1-\alpha)\|f^1\|_\infty\right).$$

(2) Proceeding as in the case of $k = 1$, when $k = 2$, we have:

$$\begin{aligned}
\|v^2\|_\infty &\le C_1 \left\{(1-b_1^{(\alpha)})\|v^1\|_\infty + b_1^{(\alpha)}\left(\|v^0\|_\infty + t_2^\alpha \Gamma(1-\alpha)\|f^2\|_\infty\right)\right\} \\
&= C_1 \left\{(1-b_1^{(\alpha)})\left(\|v^0\|_\infty + t_1^\alpha \Gamma(1-\alpha)\|f^1\|_\infty\right)\right. \\
&\quad \left. + b_1^{(\alpha)}\left(\|v^0\|_\infty + t_2^\alpha \Gamma(1-\alpha)\|f^2\|_\infty\right)\right\} \\
&\le C_1 \left\{\|v^0\|_\infty + \left[(1-b_1^{(\alpha)})t_2^\alpha + b_1^{(\alpha)} t_2^\alpha\right]\Gamma(1-\alpha)\max_{i=1,2}\|f^i\|_\infty\right\} \\
&= C_1 \left(\|v^0\|_\infty + t_2^\alpha \Gamma(1-\alpha)\max_{i=1,2}\|f^i\|_\infty\right).
\end{aligned}$$

(3) Suppose that the cases of $k = 3, 4, \ldots k-1$ for (5.4) have been proved, considering the $m^{th}(1 \le m \le k-1)$ layer, it has:

$$\|v^m\|_\infty \le \|v^0\|_\infty + t_m^\alpha \Gamma(1-\alpha)\max_{1\le k\le m}\|f^k\|_\infty.$$

Then, we can deduce the (5.4) at the $k^{th}$ layer:

$$\begin{aligned}
\|v^k\|_\infty &\le C_1 \left\{\sum_{m=1}^{k-1}\left[b_{k-m-1}^{(\alpha)} - b_{k-m}^{(\alpha)}\right]\|v^m\|_\infty + b_{k-1}^{(\alpha)}\left[\|v^0\|_\infty + t_k^\alpha \Gamma(1-\alpha)\|f^n\|_\infty\right]\right\} \\
&\le C_1 \left\{\sum_{m=1}^{k-1}\left[b_{k-m-1}^{(\alpha)} - b_{k-m}^{(\alpha)}\right]\left(\|v^0\|_\infty + t_m^\alpha \Gamma(1-\alpha)\max_{1\le k\le m}\|f^m\|_\infty\right)\right. \\
&\quad \left. + b_{n-1}^{(\alpha)}\left[\|v^0\|_\infty + t_k^\alpha \Gamma(1-\alpha)\max_{1\le n\le m}\|f^n\|_\infty\right]\right\} \\
&= C_1 \left\{\left(\sum_{m=1}^{k-1}\left[b_{k-m-1}^{(\alpha)} - b_{k-m}^{(\alpha)}\right] + b_{k-1}^{(\alpha)}\right)\|v^0\|_\infty\right. \\
&\quad \left. + \left(\sum_{m=1}^{k-1}\left[b_{k-m-1}^{(\alpha)} - b_{k-m}^{(\alpha)}\right] + b_{k-1}^{(\alpha)}\right)t_k^\alpha \Gamma(1-\alpha)\max_{1\le n\le k}\|f^n\|_\infty\right\} \\
&= C_1 \left(\|v^0\|_\infty + t_k^\alpha \Gamma(1-\alpha)\max_{1\le n\le k}\|f^n\|_\infty\right).
\end{aligned}$$

It is now obvious that the Theorem 5.1 holds. □

## 6 Convergence analysis

**Theorem 6.1** *Let $\{u_{ij}^k | (i,j) \in \omega, 1 \le k \le K\}$ be the solution of differential equations [Eqs. (2.1)–(2.3)]; let $\{U_{ij}^k | (i,j) \in \omega, 1 \le k \le K\}$ be the solution of CFDS (2.42)–(2.45). Denote:*

$$e_{ij}^k = u_{ij}^k - U_{ij}^k, \qquad (i,j) \in \omega,\ 1 \le k \le K,$$

*then there exists a positive constant $\tilde{C}$ independent of the splitting, such that:*

$$\|e^k\|_\infty \le \tilde{C}T^\alpha \Gamma(1-\alpha)(\tau^{2-\alpha} + h_1^4 + h_2^4), \qquad 1 \le k \le K. \tag{6.1}$$

***Proof*** By a comparison of (2.39)–(2.41) and (2.42)–(2.45), subtracting the corresponding equations to get the error equation:

$$\begin{aligned}
&a_1 e_{ij}^k + a_2 e_{i+1,j}^k + a_3 e_{i-1,j}^k + a_4 e_{i,j+1}^k + a_4 e_{i,j-1}^k \\
&\quad + a_5 e_{i+1,j+1}^k + a_6 e_{i-1,j+1}^k + a_5 e_{i+1,j-1}^k + a_6 e_{i-1,j-1}^k \\
&= b_1\mu \sum_{m=1}^{k-1} \left[b_{k-m-1}^{(\alpha)} - b_{k-m}^{(\alpha)}\right] e_{ij}^m + b_2\mu \sum_{m=1}^{k-1} \left[b_{k-m-1}^{(\alpha)} - b_{k-m}^{(\alpha)}\right] e_{i+1,j}^m \\
&\quad + b_3\mu \sum_{m=1}^{k-1} \left[b_{k-m-1}^{(\alpha)} - b_{k-m}^{(\alpha)}\right] e_{i-1,j}^m + b_4\mu \sum_{m=1}^{k-1} \left[b_{k-m-1}^{(\alpha)} - b_{k-m}^{(\alpha)}\right] e_{i,j+1}^m \\
&\quad + b_4\mu \sum_{m=1}^{k-1} \left[b_{k-m-1}^{(\alpha)} - b_{k-m}^{(\alpha)}\right] e_{i,j-1}^m + b_1\mu b_{k-1}^{(\alpha)} e_{ij}^0 + b_2\mu b_{k-1}^{(\alpha)} e_{i+1,j}^0 + b_3\mu b_{k-1}^{(\alpha)} e_{i-1,j}^0 \\
&\quad + b_4\mu b_{k-1}^{(\alpha)} e_{i,j+1}^0 + b_4\mu b_{k-1}^{(\alpha)} e_{i,j-1}^0 + f_{ij}^k, \qquad (i,j) \in \omega,\ 1 \le k \le K,
\end{aligned} \tag{6.2}$$

$$e_{ij}^0 = \varphi(x_i, y_j), \qquad (i,j) \in \omega, \tag{6.3}$$

$$\begin{aligned}
&e_{0,y}^k(0,y) = e_{l_1,y}^k(l_1,y) = 0, \qquad y \in (0,l_2),\ 1 \le k \le K, \\
&e_{x,0}^k(x,0) = e_{x,l_2}^k(x,l_2) = 0, \qquad x \in (0,l_1),\ 1 \le k \le K,
\end{aligned} \tag{6.4}$$

where $f_{ij}^k$ represents a small perturbation of the source term at the right end.

Applying Theorem 5.1 into (6.2)–(6.4) and using (5.4), we obtain:

$$\begin{aligned}
\|e^k\|_\infty &\le C_1 \left( \|e^0\|_\infty + t_k^\alpha \Gamma(1-\alpha) \max_{1\le n\le k} \|(\hat{R}_{ij}^k)^n\|_\infty \right) \\
&\le C_1 \left( t_k^\alpha \Gamma((1-\alpha)) C_0 (\tau^{2-\alpha} + h_1^4 + h_2^4) \right) \\
&\le \tilde{C}T^\alpha \Gamma(1-\alpha)(\tau^{2-\alpha} + h_1^4 + h_2^4), \qquad 1 \le k \le K,
\end{aligned} \tag{6.5}$$

where $\tilde{C} = C_0 \cdot C_1$. This completes the proof of Theorem 6.1. □

## 7 Numerical experiments

In this section, we carry out several numerical experiments for the fourth-order CFDS (2.42) to illustrate our theoretical analysis. We performed our computation using MATLAB 7 software environment with version R2014a on a Lenovo notebook computer, and they were executed on Inter(R) Core(TM)i7-6500U CPU @ GHz, RAM 8.00 GB (7.44 GB available). For simplicity, all examples in this paper are taken uniform step size $h_1 = h_2 = h$.

We compute the $L_2$ norm and $L_\infty$ norm errors between the numerical and the exact solutions, which are defined as follows:

$$errL_\infty = \max_{\substack{1\le i\le N_1-1\\ 1\le j\le N_2-1}} \left|U_{ij}^K - u(x_i, y_j, T)\right|,$$

$$errL_2 = \left\{ h_1 h_2 \sum_{i=1}^{N_1-1}\sum_{j=1}^{N_2-1} \left|U_{ij}^K - u(x_i, y_j, T)\right|^2 \right\}^{\frac{1}{2}}.$$

For the sufficiently small $\tau$, the spatial convergence order is denoted by:

$$Rate = \log_2\left(\frac{E(2h,\tau)}{E(h,\tau)}\right).$$

Although we study the high-order scheme of the 2D problems, the scheme (2.42) can also be applied to the 1D problems to obtain the fourth-order accuracy in spatial. Here we not only show the scheme (2.42) for the 2D problems, we perform the accuracy for 1D problems with $D_2 = 0$ and $D_1 = v = 1$. First, we consider the following 1D IBVPs with $l_1 = l_2 = T = 1$ and $N_1 = N$ to verify our statements:

$$\begin{cases} {}_0^C D_t^\alpha u(x,t) + \dfrac{\partial u(x,t)}{\partial x} - \dfrac{\partial^2 u(x,t)}{\partial x^2} = g(x,t), \quad (x,t) \in [0,1]\times[0,1], \\ u(x,0) = \varphi(x), \quad 0 \le x \le 1, \\ u(0,t) = \psi_1(t), \quad u(1,t) = \psi_2(t), \quad 0 < t \le 1. \end{cases} \tag{7.1}$$

***Example 1*** Consider (7.1) with the following homogeneous Dirichlet boundary condition:

$$\begin{cases} \varphi(x) = 0, \\ \psi_1(t) = 0, \quad \psi_2(t) = 0, \\ g(x,t) = \dfrac{t^{1-\alpha}}{\Gamma(2-\alpha)}\sin(\pi x) + t[\pi\cos(\pi x) + \pi^2\sin(\pi x)]. \end{cases} \tag{7.2}$$

The exact solution for problem (7.1) under the condition of (7.2) is:

$$u(x,t) = t\sin(\pi x). \tag{7.3}$$

For the time-fractional order $\alpha = 0.25, 0.75$, the error accuracy and convergence order of $L_2$ norm and $L_\infty$ norm between numerical solution and exact solution in spatial with $\tau = 1/50$ and $N = \{2, 4, 8, 16, 32\}$ at $t = T$ are reported in Table 1. It is obvious that the spatial convergence order is approximately 4 for each $\alpha$, which matches well with the theoretical results for Example 1.

Figure 2 plots the fitted curve and absolute error curve of numerical solution and exact solution with $\alpha = 0.25$, $h = 1/16$ and $\tau = 1/256$ when $t = T$ for Example 1. We can clearly see that the exact solution can be simulated well by the numerical solution for our scheme (2.42) with $D_2 = 0$ in this case.

***Example 2*** Consider (7.1) with the following non-homogeneous Dirichlet boundary condition:

$$\begin{cases} \varphi(x) = 0, \\ \psi_1(t) = t, \quad \psi_2(t) = t\exp(1), \\ g(x,t) = \dfrac{t^{1-\alpha}}{\Gamma(2-\alpha)}\exp(x). \end{cases} \tag{7.4}$$

**Table 1** The $L_2$ and $L_\infty$ errors with corresponding spatial orders for Example 1 when $K = 50$

| $\alpha$ | $N$ | $L_2$ error | Order | $L_\infty$ error | Order |
|---|---|---|---|---|---|
| $\alpha = 0.25$ | 2 | 1.4714e−002 | | 2.0809e−002 | |
| | 4 | 9.0438e−004 | 4.0676 | 1.2660e−003 | 4.1092 |
| | 8 | 5.6115e−005 | 4.0291 | 8.1347e−005 | 3.8907 |
| | 16 | 3.5003e−006 | 4.0078 | 5.0971e−006 | 3.9898 |
| | 32 | 2.1865e−007 | 4.0020 | 3.1941e−007 | 3.9893 |
| $\alpha = 0.75$ | 2 | 1.4614e−002 | | 2.0668e−002 | |
| | 4 | 8.9865e−004 | 4.0234 | 1.2577e−003 | 4.0385 |
| | 8 | 5.5761e−005 | 4.0104 | 8.0890e−005 | 3.9586 |
| | 16 | 3.4782e−006 | 4.0028 | 5.0662e−006 | 3.9969 |
| | 32 | 2.1727e−007 | 4.0007 | 3.1755e−007 | 3.9958 |

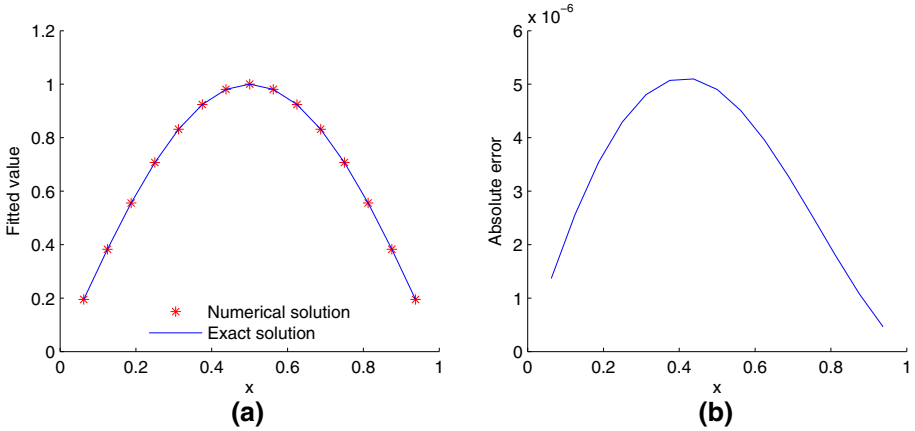


**Fig. 2** **a** Fitted figure of numerical solution and exact solution at $t = T$ with $\alpha = 0.25$ and $K = N^2 = 256$. **b** Absolute error curve between numerical solution and exact solution at $t = T$ with $\alpha = 0.25$ and $K = N^2 = 256$ for Example 1

It is clear to check that the exact solution of problem (7.1) under (7.4) is:

$$u(x, t) = t \exp(x). \tag{7.5}$$

Table 2 list the error accuracy and convergence order of $L_2$ norm and $L_\infty$ norm between numerical solution and exact solution in spatial with $\tau = 1/60$ and $N = \{4, 8, 16, 32, 64\}$ at $t = T$ for Example 2. It shows that the proposed scheme (2.22) has a good results in both error accuracy and convergence order for different time-fractional order $\alpha = 0.3, 0.9$.

In Fig. 3, the fitted curve and absolute error curve of numerical solution and exact solution of problem (7.1) are plotted with $\alpha = 0.3$, $h = 1/64$, and $\tau = 1/60$ when $t = T$ for Example 2. We observe that the numerical solution match well with the exact solution.

Figure 4 depicts convergence order and error variation of $L_2$ norm between numerical solution and exact solution for different spatial step sizes with the same parameter values as Fig. 3. It indicates the convergence order, obtained by the semi-log scale errors, which

**Table 2** The $L_2$ and $L_\infty$ errors with corresponding spatial orders for Example 2 when $K = 60$

| $\alpha$ | $N$ | $L_2$ error | Order | $L_\infty$ error | Order |
|---|---|---|---|---|---|
| $\alpha = 0.3$ | 4 | 7.3404e−007 | | 9.8781e−007 | |
| | 8 | 4.5904e−008 | 3.9991 | 6.2976e−008 | 3.9713 |
| | 16 | 2.8676e−009 | 4.0006 | 3.9520e−009 | 3.9941 |
| | 32 | 1.7922e−0010 | 4.0000 | 2.4745e−0010 | 3.9973 |
| | 64 | 1.1187e−0011 | 4.001 | 1.5446e−0011 | 4.0018 |
| $\alpha = 0.9$ | 4 | 7.3180e−007 | | 9.8465e−007 | |
| | 8 | 4.5765e−008 | 3.9991 | 6.2784e−008 | 3.9711 |
| | 16 | 2.8589e−009 | 4.0006 | 3.9396e−009 | 3.9942 |
| | 32 | 1.7864e−0010 | 4.0003 | 2.4664e−0010 | 3.9975 |
| | 64 | 1.1179e−0011 | 3.9981 | 1.5434e−0011 | 3.9981 |

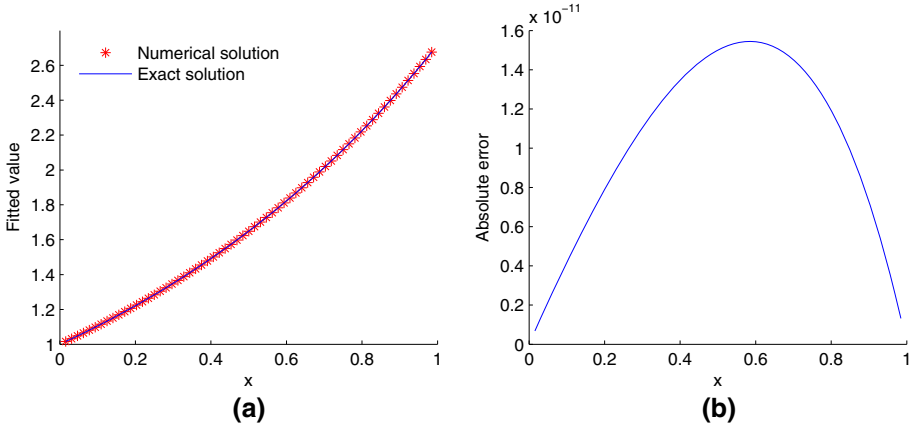


**Fig. 3** **a** Fitted figure of numerical solution and exact solution at $t = T$ with $\alpha = 0.3$, $N = 64$, and $K = 60$. **b** Absolute error curve between numerical solution and exact solution at $t = T$ with $\alpha = 0.3$, $N = 64$, and $K = 60$ for Example 2

indicates an exponential convergence rate $\mathcal{O}(h^4)$, and the $L_2$ error value gradually decreases to 0 as the number of spatial split nodes increases.

Whether it is from tables or figures, we can clearly see that the scheme (2.20) can well approximate the exact solution for the 1D problem, and its spatial convergence order reaches the fourth-order accuracy, which supports our theoretical results. Next, we turn back to the 2D IBVPs with $N_1 = N_2 = N$.

***Example 3*** Consider the 2D time-fractional convection diffusion problem (2.1) with the initial-boundary valve conditions:

$$\begin{cases} u(x, y, 0) = 0, \quad (x, y) \in \Omega, \\ u(0, y, t) = u(1, y, t) = 0, \quad y \in (0, 1), \ t \in (0, 1], \\ u(x, 0, t) = u(x, 1, t) = 0, \quad x \in (0, 1), \ t \in (0, 1], \end{cases} \tag{7.6}$$

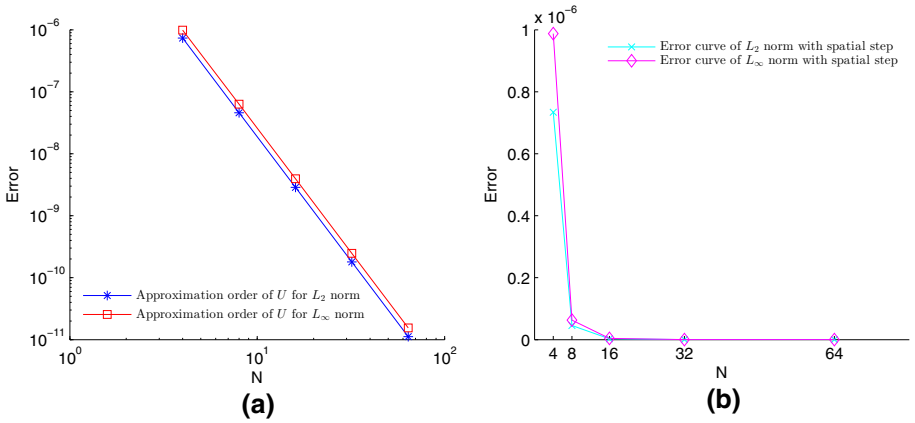


**Fig. 4** **a** Convergence orders of $L_2$ norm and $L_\infty$ norm at $t = T$ with $\alpha = 0.3$ and $K = 60$. **b** Error variation curves of $L_2$ norm and $L_\infty$ norm as different number of spatial nodes at $t = T$ with $\alpha = 0.3$ and $K = 60$ for Example 2

**Table 3** The $L_2$ and $L_\infty$ errors with corresponding spatial orders for scheme (2.42) in Example 3 when $K = 50$

| $\alpha$ | $N$ | $L_2$ error | Order | $L_\infty$ error | Order |
|---|---|---|---|---|---|
| $\alpha = 0.25$ | 4 | 5.5273e−004 | | 1.1041e−003 | |
| | 8 | 3.5571e−005 | 3.8845 | 7.1039e−005 | 3.8853 |
| | 16 | 2.2376e−006 | 3.9906 | 4.5144e−006 | 3.9759 |
| | 32 | 1.4007e−007 | 3.9977 | 2.8259e−007 | 3.9977 |
| | 64 | 8.7578e−009 | 3.9985 | 1.7690e−008 | 3.9936 |
| $\alpha = 0.75$ | 4 | 5.5156e−004 | | 1.1017e−003 | |
| | 8 | 3.5496e−005 | 3.9577 | 7.0887e−005 | 3.9581 |
| | 16 | 2.2329e−006 | 3.9906 | 4.5051e−006 | 3.9758 |
| | 32 | 1.3977e−007 | 3.9977 | 2.8202e−007 | 3.9977 |
| | 64 | 8.7392e−009 | 3.9985 | 1.7654e−008 | 3.9937 |

and source term:

$$(x, y, t) = \frac{t^{1-\alpha}}{\Gamma(2-\alpha)} \sin(\pi x)\sin(\pi y) + t\big[\pi^2(D_x + D_y)\sin(\pi x)\sin(\pi y) + \pi v \cos(\pi x)\sin(\pi y)\big]. \tag{7.7}$$

The exact solution of problem (2.1) under the conditions (7.6) and (7.7) is:

$$u(x, y, t) = t \sin(\pi x)\sin(\pi y). \tag{7.8}$$

Let $l_1 = l_2 = T = 1$ and $D_1 = D_2 = v = 1$, with different time order $\alpha = 0.25, 0.75$ and different number of spatial nodes $N = \{4, 8, 16, 32, 64\}$, and the comparison of error accuracy between $L_2$ and $L_\infty$ of numerical solution and exact solution and their corresponding spatial convergence order with $\tau = 1/50$ at $t = T$ for Example 3 are presented in Table 3. It is evident that the fourth order of convergence in spatial is apparent.

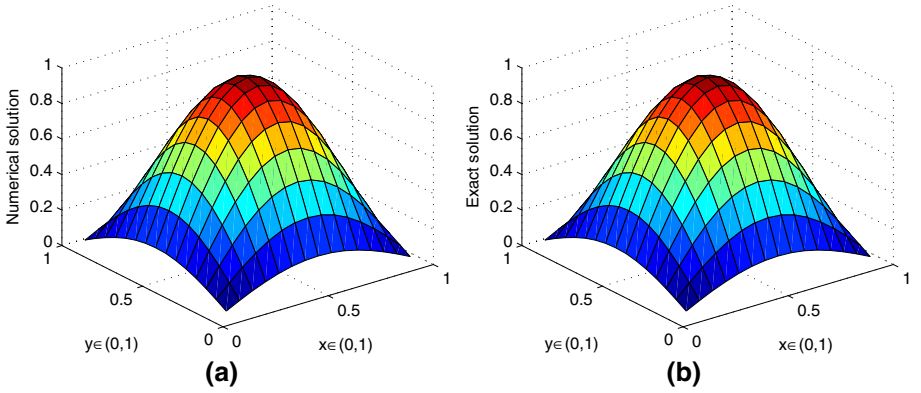


**Fig. 5** **a** Numerical solution at $t = T$ with $\alpha = 0.25$, $N = 16$, and $K = 50$. **b** Exact solution at $t = T$ with $\alpha = 0.25$, $N = 16$, and $K = 50$ for Example 3

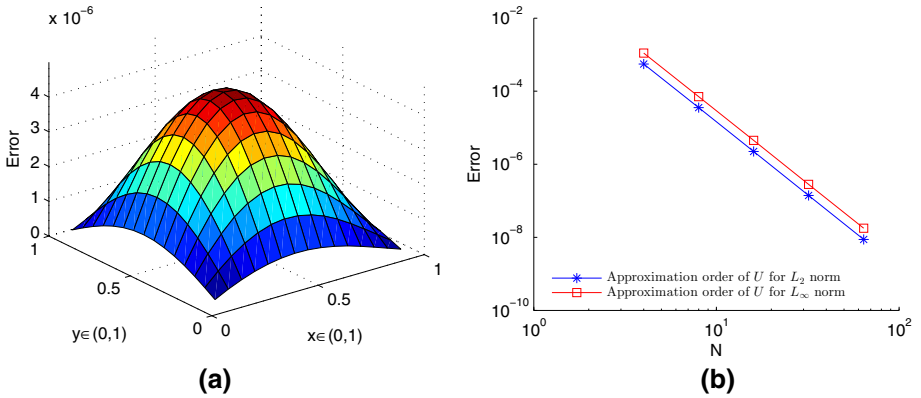


**Fig. 6** **a** Absolute error figure between numerical solution and exact solution at $t = T$ with $\alpha = 0.25$, $N = 16$ and $K = 50$. **b** Convergence orders of $L_2$ norm and $L_\infty$ norm at $t = T$ with $\alpha = 0.25$, $N = 16$, and $K = 50$ for Example 3

In Fig. 5, we draw the surface figures of numerical solution and exact solution with $\alpha = 0.25$, $N = 16$, and $K = 50$ at the last time layer, respectively. From it, we can find that our numerical method can solve well the numerical solution in this case for Example 3.

In Fig. 6, we give the error surface figure for $|u - U|$ and convergence order curve for different spatial step sizes with $\alpha = 0.25$, $N = 16$, $K = 50$ and $t = T$. we can clearly see that the scheme (2.42) gives a good approximation of the 2D problem (2.1), and its local truncation error in spatial is $\mathcal{O}(h_1^4 + h_2^4)$, which is consistent with theoretical analysis.

***Example 4*** Consider the 2D time-fractional convect–diffusion equation (2.1) in (Li et al. 2013) with zero initial-boundary valve conditions (7.6) and source term:

$$g(x, y, t) = \frac{t^{1-\alpha}}{\Gamma(2-\alpha)} xy(x-1)(y-1) - 2D_1 ty(y-1) - 2D_2 tx(x-1) + vt(2x-1)y.(y-1), \quad (7.9)$$

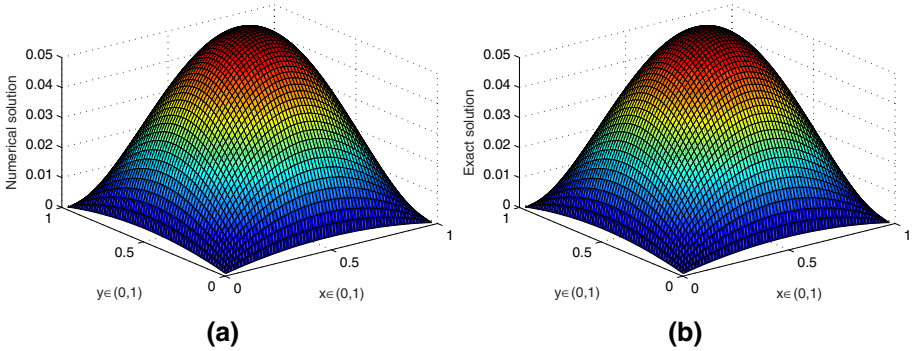


**Fig. 7** **a** Numerical solution at $T = 1$ with $\alpha = 0.3$, $N = 64$, and $K = 50$. **b** Exact solution at $T = 1$ with $\alpha = 0.3$, $N = 64$, and $K = 50$ for Example 4

**Table 4** Comparison of numerical solution and absolute error with different $(x, y)$ at $t = T$ for Example 4

| $x$ | $y$ | Exact solution | Numerical solution | Absolute error | Numerical solution in (Li et al. 2013) | Absolute error in (Li et al. 2013) |
|---|---|---|---|---|---|---|
| 0.1 | 0.1 | 0.0081 | 0.0081 | 8.6736e−0018 | 0.0080 | 6.7702e−005 |
| 0.2 | 0.2 | 0.0256 | 0.0256 | 2.4286e−0017 | 0.0255 | 9.6522e−005 |
| 0.3 | 0.3 | 0.0441 | 0.0441 | 3.4694e−0017 | 0.0440 | 6.9271e−005 |
| 0.4 | 0.4 | 0.0576 | 0.0576 | 2.7755e−0017 | 0.0575 | 8.4309e−005 |
| 0.5 | 0.5 | 0.0625 | 0.0625 | 6.9388e−0017 | 0.0624 | 9.0775e−005 |
| 0.6 | 0.6 | 0.0576 | 0.0576 | 7.6327e−0017 | 0.0575 | 8.4334e−005 |
| 0.7 | 0.7 | 0.0441 | 0.0441 | 4.8572e−0017 | 0.0440 | 6.6275e−005 |
| 0.8 | 0.8 | 0.0256 | 0.0256 | 3.4694e−0017 | 0.0256 | 4.1243e−005 |
| 0.9 | 0.9 | 0.0081 | 0.0081 | 8.6736e−0018 | 0.0080 | 9.6006e−005 |

Such that the exact solution of problem (2.1) under (7.6) and (7.9) is:

$$u(x, y, t) = txy(x - 1)(y - 1). \tag{7.10}$$

Let $l_1 = l_2 = T = 1$ and $D_1 = D_2 = 1$, $v = 0.001$, and Fig. 7 gives the surface figures of numerical solution and exact solution derived from the fourth-order CFDS (2.42) for (2.1) with $N_1 = N_2 = 64$, $K = 50$ and $\alpha = 0.3$. It can be seen that numerical solution and exact solution fit very well.

Table 4 gives the numerical comparison results at different locations $(x, y)$ of CFDS (2.42) we designed and general difference scheme proposed by (Li et al. 2013) with discrete nodes $N_1 = N_2 = 10$, $K = 100$, time-differential order $\alpha = 0.6$, diffusion coefficients $D_1 = D_2 = v = 0.001$, and convection velocity $v = 0.001$. We can see that the error of (2.42) is more smaller than (Li et al. 2013), and the convergence order is more higher.

Table 5 lists the numerical comparison results under different times ($t = 0.1, 0.2, \ldots, 0.9$) of CFDS (2.42) and general difference scheme (Li et al. 2013) at the location (0.5, 0.5) with $N_1 = N_2 = 10$, $K = 100$, $\alpha = 0.6$, $D_1 = D_2 = v = 0.001$, respectively. Corresponding, with the same parameter value as Tables 5 and 6 gives the numerical comparison results under different differential orders ($\alpha = 0.1, 0.2, \ldots, 0.9$) of CFDS (2.42) and general difference

**Table 5** Comparison of numerical solution and absolute error for Example 3 with different $t$ values at $\alpha = 0.6$ and $(x = y = 0.5)$

| $t$ | Exact solution | Numerical solution | Absolute error | Relative error | Numerical solution in Li et al. (2013) | Absolute error in Li et al. (2013) | Relative error in Li et al. (2013) |
|---|---|---|---|---|---|---|---|
| 0.1 | 0.0063 | 0.0063 | 0 | 0 | 0.0062 | 7.9169e−006 | 0.0013 |
| 0.2 | 0.0125 | 0.0125 | 0 | 0 | 0.0125 | 1.6236e−005 | 0.0013 |
| 0.3 | 0.0187 | 0.0188 | 6.9388e−0018 | 1.5860e−0016 | 0.0187 | 2.4843e−005 | 0.0013 |
| 0.4 | 0.0250 | 0.0250 | 1.3877e−0017 | 3.7007e−0016 | 0.0250 | 3.3691e−005 | 0.0013 |
| 0.5 | 0.0313 | 0.0313 | 6.9388e−0018 | 2.2204e−0016 | 0.0312 | 4.2754e−005 | 0.0014 |
| 0.6 | 0.0375 | 0.0375 | 3.4694e−0018 | 1.3877e−0016 | 0.0374 | 5.2014e−005 | 0.0014 |
| 0.7 | 0.0437 | 0.0438 | 6.9388e−0018 | 3.7007e−0016 | 0.0437 | 6.1456e−005 | 0.0014 |
| 0.8 | 0.0500 | 0.0500 | 1.7347e−0018 | 1.3877e−0016 | 0.0499 | 7.1069e−005 | 0.0014 |
| 0.9 | 0.0563 | 0.0563 | 8.6736e−0019 | 1.3877e−0016 | 0.0562 | 8.0845e−005 | 0.0014 |

**Table 6** Comparison of numerical solution and absolute error of Example 3 with different $\alpha$ values at $t = T = 1$ and $(x = y = 0.5)$

| $\alpha$ | Exact solution | Numerical solution | Absolute error | Relative error | Numerical solution in Li et al. (2013) | Absolute error in Li et al. (2013) | Relative error in Li et al. (2013) |
|---|---|---|---|---|---|---|---|
| 0.1 | 0.0625 | 0.0625 | 6.9388e−0018 | 1.1102e−0016 | 0.0625 | 2.4839e−005 | 3.9742e−004 |
| 0.2 | 0.0625 | 0.0625 | 1.3877e−0017 | 2.2204e−0016 | 0.0625 | 2.6175e−005 | 4.1880e−004 |
| 0.3 | 0.0625 | 0.0625 | 6.9388e−0018 | 1.1102e−0016 | 0.0625 | 3.0270e−005 | 4.8436e−004 |
| 0.4 | 0.0625 | 0.0625 | 1.3877e−0017 | 2.2204e−0016 | 0.0625 | 3.9475e−005 | 6.3159e−004 |
| 0.5 | 0.0625 | 0.0625 | 0 | 0 | 0.0624 | 5.7621e−005 | 9.2194e−004 |
| 0.6 | 0.0625 | 0.0625 | 1.3877e−0017 | 2.2204e−0016 | 0.0624 | 9.0775e−005 | 0.0015 |
| 0.7 | 0.0625 | 0.0625 | 4.1633e−0017 | 6.6613e−0016 | 0.0624 | 1.4815e−004 | 0.0024 |
| 0.8 | 0.0625 | 0.0625 | 0 | 0 | 0.0623 | 2.4319e−004 | 0.0039 |
| 0.9 | 0.0625 | 0.0625 | 2.7755e−0017 | 4.4408e−0016 | 0.0621 | 3.9465e−004 | 0.0063 |

scheme (Li et al. 2013) at the location (0.5, 0.5), respectively. It can be seen that the numerical solution of (Li et al. 2013) agrees well with exact solution at the given spatial coordinate $(x, y)$, but the accuracy is still lower than our method. It shows that our fourth-order compact difference scheme (2.42) owns the better approximation effect for practical problems.

As can be seen from the Table 6, for (Li et al. 2013), the time differential order $\alpha$ has certain influence on solving the problem (2.1). The smaller the differential order $\alpha$, the smaller the error between numerical solution and exact solution. When $\alpha$ closing to 1, the error increases gradually. For our method, the monotonicity effect is not so significant comparing with (Li et al. 2013), but it is enough to show that the fourth-order compact difference scheme (2.42) has good approximation accuracy.

Last but not least, when $N_1 = N_2 = 10$, $K = 100$, $\alpha = 0.6$, $D_1 = D_2 = v = 0.001$, the $L_2$ norm error of scheme (2.42) is 2.5091e-0017, $L_\infty$ norm error is 7.6327e-0017, and both of them are very close to 0. This shows that the method which we proposed is more superior, and the simulation data of the practical problem are more accurate.

In the above four experiments, we verified the validity of the proposed numerical scheme (2.42) by constructing exact solutions. However, for most groundwater pollution problems in engineering, we have no exact solution at all. So far, we can only solve the corresponding IBVP numerically to get pollutant concentration. With the above theoretical basis and example verification, we will use our models and methods to perform numerical simulation on practical problem of groundwater pollution.

***Example 5*** Consider the practical problem (2.1) for the case of an instantaneous release of groundwater pollutant. There is an initial amount of pollution at the source of pollution, the initial condition can be described using a 2D $\delta$-distribution, and the boundary conditions can be expressed as the limit of the concentration of pollutant at infinity:

$$\begin{cases} u(x, y, 0) = \delta(x)\delta(y), \quad (x, y) \in \Omega, \\ \lim_{x\to\pm\infty} u(x, y, t) = 0, \quad y \in (0, l_2),\ t \in (0, T], \\ \lim_{y\to\pm\infty} u(x, y, t) = 0, \quad x \in (0, l_1),\ t \in (0, T]. \end{cases} \tag{7.11}$$

Let $l_1 = l_2 = 20$, $N_1 = N_2 = 20$, $K = 10$, convection velocity $v = 1$, and diffusion coefficients $D_1 = D_2 = 1$, and we visualize the behaviour of numerical solution and the corresponding aerial perspective figure when $\alpha = 0.5$ in Fig. 8. Obviously, when the order of time-fractional derivative is fixed, the longer times, the lower the pollution concentration peak occurs.

Figure 8 demonstrates simulation concentration for the time are chosen $t = 10$, $t = 30$, and $t = 50$, respectively. From a fluid mechanics perspective, due to the existence of the time-fractional derivative that describes the slow-diffusion phenomenon, the migration speed of the pollutants in the $x$-axis direction is significantly reduced. In other words, the time-fractional derivative reduces the pollutants convection velocity to a certain extent, which is consistent with the seepage phenomenon in complex media. In addition, it is worth noting that while the pollutants are moving along the $x$-axis, they also diffuse in the $x$-axis and $y$-axis directions. The increase in both directions simultaneously increases the area of the area affected by pollutants. That is to say, time-fractional derivative increases the influence of diffusion to convection during pollutant transport.

The above analysis shows that the pollution area caused by the slow-diffusion phenomenon occurs not far from the pollution source, and it will not have a serious impact on the downstream water quality for a considerable period of time. Therefore, we can con-

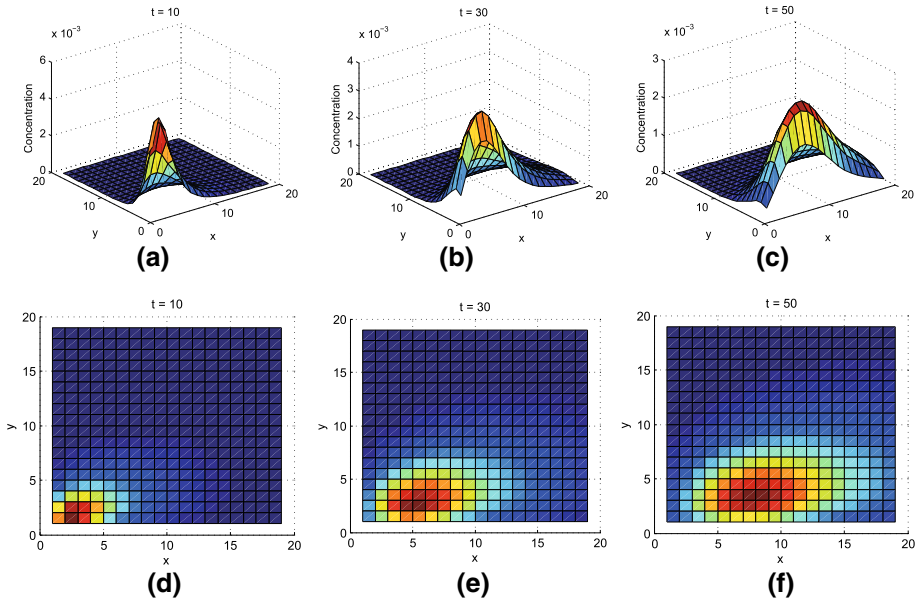


**Fig. 8** **a–c** Numerical solution figures at $t = 10$, $t = 30$, and $t = 50$ when $\alpha = 0.5$. **d–f** Corresponding 2D aerial perspective figures for Example 5

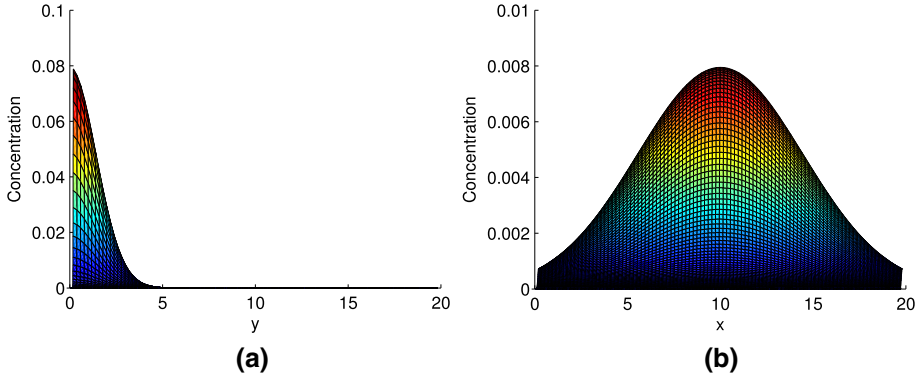


**Fig. 9** **a** The duration of pollution diffusion in $y$-axis direction simulated at $t = 0$s. **b** The duration of pollution diffusion in $x$-axis direction simulated at $t = 10$s for Example 5

trol the contaminated water sources accordingly to avoid causing greater economic losses to society.

Figure 9 shows two different aspects of pollution diffusion by sketch the diffusive progress from the $x$-axis and $y$-axis point of view. The different colors mark the different concentration values of pollution. From the comparison studies of the duration in two directions, we find that the $x$-axis figure shows the convection of the concentration peak moving from $x = 0$ at the beginning to $x = 10$ at the end, but the peak of $y$-axis figure one curve is still at $y = 0$, because there is no velocity along the $y$-axis direction.

Furthermore, we compare the simulation concentration with different order of time-fractional derivative when $t = 10$. We recognize that the parameter $\alpha$ has great impacts

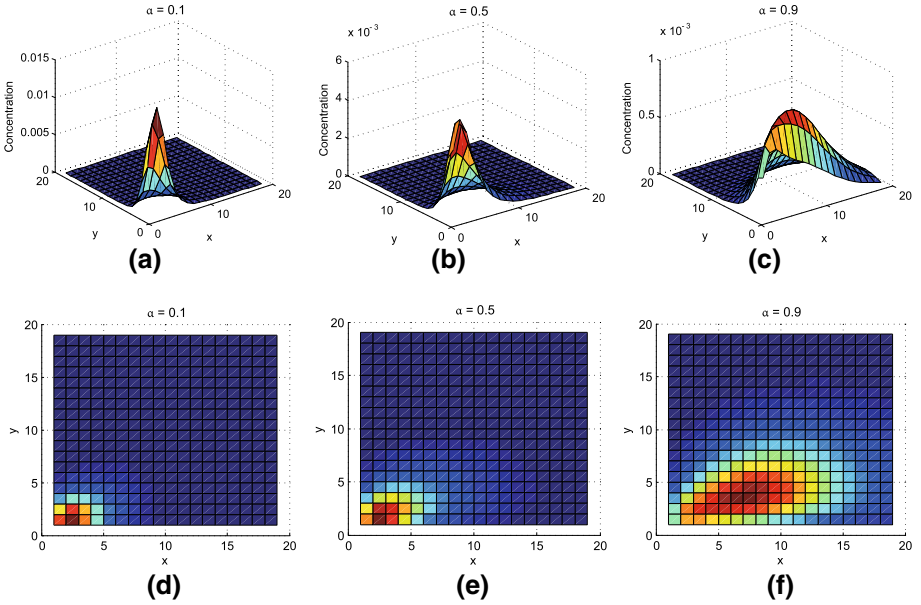


**Fig. 10** **a–c** Numerical solution figures at $\alpha = 0.1$, $\alpha = 0.5$, and $\alpha = 0.9$ when $t = 10$. **d–f** Corresponding 2D aerial perspective figures for Example 5

on the solution of pollutants concentration. Figure 10 shows the numerical solution and the corresponding 2D aerial perspective figures of concentration with $\alpha = 0.1$, $\alpha = 0.5$, and $\alpha = 0.9$ when $t = 10$.

By setting up different $\alpha$ values, Fig. 10 records the concentration values and aerial perspective figures. Similar to Fig. 8, the order $\alpha$ of the time-fractional derivative has an effect on the concentration of the pollutants. The larger the order, the lower the concentration. It shows that the parameter $\alpha$ does has an effect on slowing down the diffusion of pollutants. Obviously, when the value of $\alpha$ is smaller, the diffusion of pollutants is slower, and the most of pollutants stay near the pollution source. This property is not available in ordinary CDE. Moreover, the change trend of the Fig. 10a–c shows that even if the change step of $\alpha$ is the same (the change of $\alpha$ is 0.4 in the two adjacent pictures), a larger value of $\alpha$ has a larger 'contribution' to the polluted area. Particularly, the closer $\alpha$ to 1, the more obvious the effects of convection and diffusion. To better compare the effects of fractional and integer orders on pollutant diffusion, in next example, we will discuss problem (2.1), with $\alpha = 1$, under the conditions (7.11).

***Example 6*** Consider problem (2.1) with $\alpha = 1$ (Winkler et al. 2015). Assume that the mass of the pollutant is 1 unit; the exact solution of problem (2.1) under the conditions (7.11) is:

$$u(x, y, t) = \frac{1}{4\pi t\sqrt{D_1 D_2}} \cdot \exp\left[-\frac{(x - vt)^2}{4D_1 t} - \frac{y^2}{4D_2 t}\right]. \tag{7.12}$$

Let $l_1 = l_2 = 20$, $N_1 = N_2 = 100$, $K = 10$, convection velocity $v = 1$, and diffusion coefficients $D_1 = D_2 = 1$, and we visualize the behaviour of numerical solution and exact solution and the corresponding aerial perspective figures over different time values in Figs. 11, 12 and 13 for the simulation time are chosen $t = 5$, $t = 10$ and $t = 15$, respectively. The three correspondent figures show the concentration as a function of $x$ and $y$ at a fixed time.

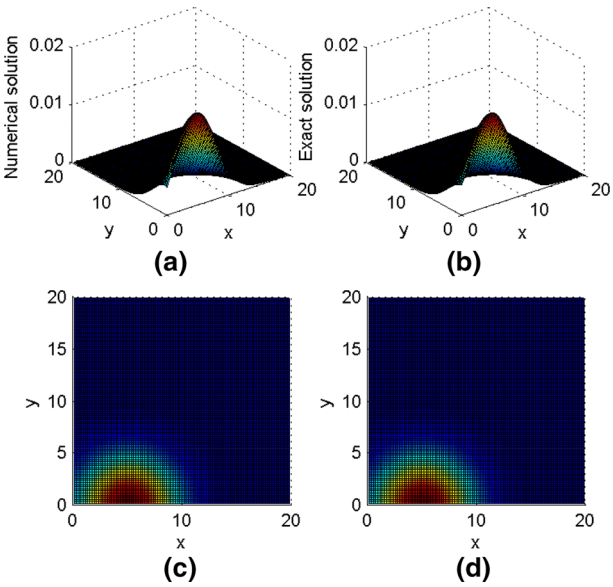


**Fig. 11** **a** Numerical solution at $t = 5$. **b** Exact solution at $t = 5$. **c** is the 2D aerial perspective figure of **a**. **d** is the 2D aerial perspective figure of **b** for Example 6

Clearly, the movement according to the flux along the $x$-axis is obvious. Differently, the peak in Fig. 11 is located at $x = 5$, for Fig. 12 at $x = 10$ and for Fig. 13 at $x = 15$. As expected, the influence of the diffusion coefficient is visible, too. Although the three figures show different scales on $z$-axis, the height values can be given. The choice of the parameter shows a good balance between convective and diffusive transport.

More precisely, Table 7 shows the numerical comparison results of CFDS (2.42) and the ordinary difference scheme in Winkler et al. (2015), including $L_2$ error, $L_\infty$ error, and peak of pollution diffusion concentration, under different times and different locations. The peak of concentration starts at 1.5884e−002, goes to 7.9498e−003, goes to 5.3016e−003 again, and ends at 3.9749e−003. All other parameters are set the same as previously used. As shown, the errors evaluated by our scheme (2.42) are significantly smaller than (Winkler et al. 2015), which shows that CFDS (2.42) is more effective for solving groundwater pollution problems.

## 8 Conclusions

In our work, CFDS with fourth order in spatial for solving 2D TF-CDE by DRT was developed. The time-fractional derivative of mentioned equation is approximated by $L_1$ interpolation approximation with order $(2-\alpha)$, $0 < \alpha < 1$, and spatial derivatives are replaced with a fourth-order CFDS. Besides, we proved the unique solvability, unconditional stability, and convergence with convergence order $\mathcal{O}(\tau^{2-\alpha} + h_1^4 + h_2^4)$. The results of numerical examples confirmed that the proposed scheme has fourth-order accuracy in spatial, which is according to theoretical results. All in all, compared with the other literatures, for the problem of groundwater pollution, the method proposed in this paper has absolute advantages in terms of convergence of solution and accuracy of pollutant concentration.

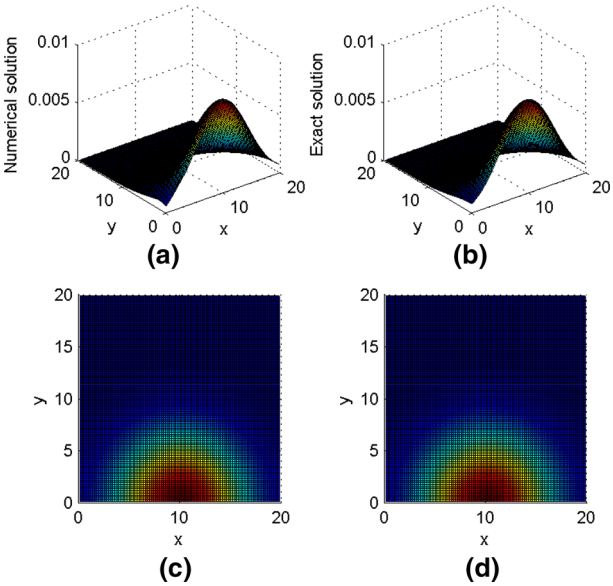


**Fig. 12** **a** Numerical solution at $t = 10$. **b** Exact solution at $t = 10$. **c** 2D aerial perspective figure of **a**. **d** 2D aerial perspective figure of **b** for Example 6

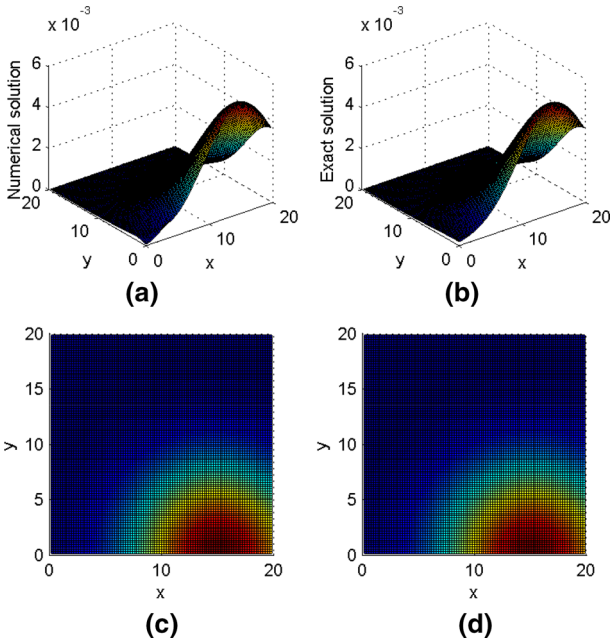


**Fig. 13** **a** Numerical solution at $t = 15$. **b** Exact solution at $t = 15$. **c** 2D aerial perspective figure of **a**. **d** 2D aerial perspective figure of **b** for Example 6

**Table 7** Numerical simulation of pollution concentration at different times and locations for Example 6

| $t$ | $(x, y)$ | $L_2$ error | $L_\infty$ error | $L_\infty$ error in Winkler et al. (2015) | Peak |
|---|---|---|---|---|---|
| 5 | (0, 5) | 3.0994e−004 | 3.2465e−004 | 7.1027e−002 | 1.5884e−002 |
| 10 | (0, 10) | 4.2273e−004 | 1.6333e−004 | 3.8183e−002 | 7.9498e−003 |
| 15 | (0, 15) | 4.3469e−004 | 1.0968e−004 | 2.6684e−002 | 5.3016e−003 |
| 20 | (0, 20) | 3.5003e−004 | 8.5070e−005 | 2.0765e−002 | 3.9749e−003 |

**Acknowledgements** The authors are very grateful to Dr. Haili Qiao of Shandong University for her assistance in the process of numerical calculation. We are also very grateful to the anonymous reviewers for their invaluable time and insightful comments leading to the improved manuscript.

**Funding** This work was partially supported by the National Natural Science Foundation of China (NSFC) under Grant Numbers 11501335 and 11371229, and the Natural Science Foundation of Shandong Province, China under Grant Numbers ZR2017MA020, ZR2017MA003.

## Compliance with ethical standards

**Conflict of interest** The authors declare that they have no conflict of interest.

## References

Augeraud-Véron E, Choquet C, Comte É (2017) Optimal control for a groundwater pollution ruled by a convection–diffusion–reaction problem. J Optim Theory Appl 173(3):941–966

Cao F, Yuan D, Ge Y (2018) The adaptive mesh method based on hoc difference scheme for convection diffusion equations with boundary layers. Comput Appl Math 37(2):1581–1600

Chang A, Sun H, Zheng C, Lu B, Lu C, Ma R, Zhang Y (2018) A time fractional convection–diffusion equation to model gas transport through heterogeneous soil and gas reservoirs. Physica A Stat Mech Appl 502:356–369

Chen C, Liu H, Zheng X, Wang H (2019) A two-grid mmoc finite element method for nonlinear variable-order time-fractional mobile/immobile advection-diffusion equations. Comput Math Appl 79(9):2771–2783

Cortis A, Gallo C, Scher H, Berkowitz B (2004) Numerical simulation of non-fickian transport in geological formations with multiple-scale heterogeneities. Water Resour Res 40(4):239–261

Cui M (2015) Compact exponential scheme for the time fractional convection–diffusion reaction equation with variable coefficients. J Comput Phys 280:143–163

Ercan A (2020) Self-similarity in fate and transport of contaminants in groundwater. Sci Total Environ 706:135738

Esquivel JM, Morales GP, Esteller MV (2015) Groundwater monitoring network design using gis and multi-criteria analysis. Water Resour Manag 29(9):3175–3194

Ewing RE, Wang H (1994) Eulerian-lagrangian localized adjoint methods for variable-coefficient advective-diffusive-reactive equations in groundwater contaminant transport. In: Gomez S, Hennart JP (eds) Advances in Optimization and Numerical Analysis. Mathematics and Its Applications, vol 275. Springer, Dordrecht

Fatoorehchi H, Abolghasemi H (2014) Finding all real roots of a polynomial by matrix algebra and the adomian decomposition method. J Egypt Math Soc 22(3):524–528

Feingold DG, Varga RS et al (1962) Block diagonally dominant matrices and generalizations of the gerschgorin circle theorem. Pacific J Math 12(4):1241–1250

Fried JJ (1975) Groundwater pollution: theory, methodology, modelling and practical rules. Elsevier, Amsterdam

Gao G, Sun Z, Zhang H (2014) A new fractional numerical differentiation formula to approximate the caputo fractional derivative and its applications. J Comput Phys 259:33–50

Gershgorin SA (1931) über die abgrenzung der eigenwerte einer matrix. Bulletin de l'Académie des Sciences de l'URSS Classe des sciences mathématiques et na 6:749–754

Gong W, Hu W, Mateos M, Singler J, Zhang X, Zhang Y (2018) A new hdg method for dirichlet boundary control of convection diffusion pdes ii: low regularity. SIAM J Numer Anal 56(4):2262–2287
Günerhan H (2020) Analytical and approximate solution of two-dimensional convection–diffusion problems. Int J Optim Control Theor Appl (IJOCTA) 10(1):73–77
Jin B, Lazarov R, Zhou Z (2016) A petrov–galerkin finite element method for fractional convection–diffusion equations. SIAM J Numer Anal 54(1):481–503
Kinzelbach W (1990) Simulation of pollutant transport in groundwater with the random walk method. Groundw Monit Manag 173:265–279
Kovarik K (2000) Numerical models in groundwater pollution. Springer, Berlin, Heidelberg
Li C, Zeng F (2012) Finite difference methods for fractional differential equations. Int J Bifurca Chaos 22(04):1230014
Li G, Gu W, Jia X (2012) Numerical inversions for space-dependent diffusion coefficient in the time fractional diffusion equation. J Inverse Ill Posed Prob 20(3):339–366
Li H, Li G, Jia X, Chi G (2013) Numerical determination of multi-point sources magnitude in 2-d time fractional advection–dispersion equation. J Shandong Univ Technol (Nal Sci Ed) 27(6):1–6 (in Chinese)
Li L, Yin Z (2017) Numerical simulation of groundwater pollution problems based on convection diffusion equation. Am J Comput Math 7(3):350–370
Li L, Jiang Z, Yin Z (2018) Fourth-order compact finite difference method for solving two-dimensional convection–diffusion equation. Adv Differ Equ 1:234
Li X, Xu C (2009) A space-time spectral method for the time fractional diffusion equation. SIAM J Numer Anal 47(3):2108–2131
Li X, Li D, Xu Y, Feng X (2020) A dfn based 3d numerical approach for modeling coupled groundwater flow and solute transport in fractured rock mass. Int J Heat and Mass Transf 149:119179
Liang D, Zhao W (1997) A high-order upwind method for the convection–diffusion problem. Comput Methods Appl Mech Eng 147(1–2):105–115
Lin Y, Xu C (2007) Finite difference/spectral approximations for the time-fractional diffusion equation. J Comput Phys 225(2):1533–1552
Logan J, Zlotnik V (1995) The convection–diffusion equation with periodic boundary conditions. Appl Math Lett 8(3):55–61
Machiwal D, Cloutier V, Güler C, Kazakis N (2018) A review of gis-integrated statistical techniques for groundwater quality evaluation and protection. Environ Earth Sci 77(19):681
Mohebbi A, Abbaszadeh M (2013) Compact finite difference scheme for the solution of time fractional advection–dispersion equation. Numer Algorithms 63(3):431–452
Munyakazi JB (2015) A uniformly convergent nonstandard finite difference scheme for a system of convection–diffusion equations. Comput Appl Math 34(3):1153–1165
NeZheng (2014) Mathematical Modeling of Groundwater Pollution. Springer, New York
Qiu W, Shi K (2016) An hdg method for convection diffusion equation. J Sci Comput 66(1):346–357
Rap A, Elliott L, Ingham D, Lesnic D, Wen X (2007) The inverse source problem for the variable coefficients convection–diffusion equation. Inverse Prob Sci Eng 15(5):413–440
Sari M, Güraslan G, Zeytinoğlu A (2010) High-order finite difference schemes for solving the advection–diffusion equation. Math Comput Appl 15(3):449–460
Shih Y, Rei C, Wang H (2009) A novel pde based image restoration: convection–diffusion equation for image denoising. J Comput Appl Math 231(2):771–779
Smaoui H, Zouhri L, Ouahsine A (2008) Flux-limiting techniques for simulation of pollutant transport in porous media: application to groundwater management. Math Comput Model 47(1–2):47–59
Srivastava PK, Han D, Gupta M, Mukherjee S (2012) Integrated framework for monitoring groundwater pollution using a geographical information system and multivariate analysis. Hydrol Sci J 57(7):1453–1472
Subramani T, Krishnamurthi P (2014) Geostatical modelling for ground water pollution in salem by using gis. Int J Engi Res Appl 4(6):165–172
Sun H, Chen W, Sze K (2013) A semi-discrete finite element method for a class of time-fractional diffusion equations. Philos Trans R Soc A Math Physi Eng Sci 371(1990):20120268
Sun N (1989) Mathematical models and numerical methods in groundwater pollution. Geological Publishing House, Beijing (in Chinese)
Sun NZ, Yeh WWG (1983) A proposed upstream weight numerical method for simulating pollutant transport in groundwater. Water Resour Res 19(6):1489–1500
Sun ZZ, Gao GH (2015) Finite difference methods for fractional differential equations. Science Press, Beijing (In Chinese)
Taghavi A, Babaei A, Mohammadpour A (2017) A coupled method for solving a class of time fractional convection–diffusion equations with variable coefficients. Comput Math Model 28(1):109–117

Wang H, Ewing R (1995) Optimal-order convergence rates for eulerian–lagrangian localized adjoint methods for reactive transport and contamination in groundwater. Numer Methods Partial Differ Equ 11(1):1–31
Wang Z, Vong S (2014) A high-order exponential adi scheme for two dimensional time fractional convection–diffusion equations. Comput Math Appl 68(3):185–196
Winkler S, Bicher M, Breitenecker F (2015) Alternative approaches for groundwater pollution. IFAC PapersOnLine 48(1):159–164
Wu L, Zhai S (2019) A new high order adi numerical difference formula for time-fractional convection–diffusion equation. Appl Math Comput:124564
Xu Q, Hesthaven JS (2014) Discontinuous galerkin method for fractional convection–diffusion equations. SIAM J Numer Anal 52(1):405–423
Yadav R, Jaiswal DK, Yadav HK, Rana G (2010) One-dimensional temporally dependent advection–dispersion equation in porous media: analysical solution. Natl Resour Model 23(4):521–539
Yu C, Wang H, Zx Wu, Wj Sun, Fatahi B (2019) Analytical solution for pollutant diffusion in soils with time-dependent dispersion coefficient. Int J Geomech 19(10):04019109
Yuan Y, Cui M, Li C, Sun T (2019) The method of mixed volume element-characteristic mixed volume element and its numerical analysis for groundwater pollution in binary medium. Appl Math Computat 362:124536
Zhang J, Zhang X, Yang B (2018) An approximation scheme for the time fractional convection–diffusion equation. Appli Math Comput 335:305–312
Zhou F, Xu X (2016) The third kind chebyshev wavelets collocation method for solving the time-fractional convection diffusion equations with variable coefficients. Appl Math Comput 280:11–29
Zhu Q, Wang Q, Fu J, Zhang Z (2012) New second-order finite difference scheme for the problem of contaminant in groundwater flow. J Appl Math 2012:1–13